

Accepted Manuscript

Structural evolution induced by substitution of designated molybdate sites (MoO_4^{-2}) with different anionic groups (BO_3^{-3} , PO_4^{-3} and SO_4^{-2}) in $\text{CaMoO}_4:\text{Sm}^{3+}$ phosphors-A study on color tunable luminescent properties



A. Balakrishna, H.C. Swart, R. Ramaraghavulu, A.K. Bedyal, R.E. Kroon, O.M. Ntwaeaborwa

PII: S0925-8388(17)32846-3

DOI: [10.1016/j.jallcom.2017.08.117](https://doi.org/10.1016/j.jallcom.2017.08.117)

Reference: JALCOM 42874

To appear in: *Journal of Alloys and Compounds*

Received Date: 14 June 2017

Revised Date: 9 August 2017

Accepted Date: 13 August 2017

Please cite this article as: A. Balakrishna, H.C. Swart, R. Ramaraghavulu, A.K. Bedyal, R.E. Kroon, O.M. Ntwaeaborwa, Structural evolution induced by substitution of designated molybdate sites (MoO_4^{-2}) with different anionic groups (BO_3^{-3} , PO_4^{-3} and SO_4^{-2}) in $\text{CaMoO}_4:\text{Sm}^{3+}$ phosphors-A study on color tunable luminescent properties, *Journal of Alloys and Compounds* (2017), doi: 10.1016/j.jallcom.2017.08.117.

This is a PDF file of an unedited manuscript that has been accepted for publication. As a service to our customers we are providing this early version of the manuscript. The manuscript will undergo copyediting, typesetting, and review of the resulting proof before it is published in its final form. Please note that during the production process errors may be discovered which could affect the content, and all legal disclaimers that apply to the journal pertain.

Structural evolution induced by substitution of designated molybdate sites (MoO_4^{-2}) with different anionic groups (BO_3^{-3} , PO_4^{-3} and SO_4^{-2}) in $\text{CaMoO}_4:\text{Sm}^{3+}$ phosphors-A study on color tunable luminescent properties

A. Balakrishna^{1*}, H.C. Swart^{1*}, R. Ramaraghavulu³, A.K. Bedyal¹, R.E. Kroon¹, O.M. Ntwaeaborwa^{2*}

¹Department of Physics, University of the Free State, Bloemfontein, ZA-9300

²School of Physics, University of the Witwatersrand, Private Bag 3, Wits, 2050, South Africa

³Department of Materials Science and Engineering, Korea University, Anam-ro, Seoul, 02841, South Korea

Abstract

A series of novel red emitting $\text{CaMoO}_4:\text{Sm}^{3+}$ (1.0 mol %) phosphors substituted with different anionic groups (BO_3^{-3} , PO_4^{-3} and SO_4^{-2}) were prepared using a high temperature solid state reaction method. The effects of anionic substitution on the crystalline structure and photoluminescence (PL) properties of the $\text{CaMoO}_4:\text{Sm}^{3+}$, $\text{CaMoO}_4\text{-BO}_3:\text{Sm}^{3+}$, $\text{CaMoO}_4\text{-PO}_4:\text{Sm}^{3+}$ and $\text{CaMoO}_4\text{-SO}_4:\text{Sm}^{3+}$ phosphors were investigated. The structure, particle morphology, chemical composition, vibration modes, and PL properties of the phosphors were investigated by X-ray diffraction (XRD), Field emission scanning electron microscopy (FE-SEM), energy dispersive spectroscopy (EDS), Fourier transform infrared spectrometry (FT-IR) and PL spectroscopy, respectively. The XRD patterns indicated that the crystalline structures of all the samples were consistent with the standard scheelite structure of CaMoO_4 . The structural parameters of the pure phase of $\text{CaMoO}_4:\text{Sm}^{3+}$ phosphor were obtained from the Rietveld analysis. Red PL attributed to the $^4\text{G}_{5/2} \rightarrow ^6\text{H}_{9/2}$ transition of Sm^{3+} was observed at 646 nm when the $\text{CaMoO}_4:\text{Sm}^{3+}$ samples were excited by 404 nm using a monochromatized Xenon lamp. Furthermore, orange-red color tunable emission has been achieved by substitution of different anionic groups (BO_3^{-3} , PO_4^{-3} and SO_4^{-2}) into the $\text{CaMoO}_4:\text{Sm}^{3+}$ phosphors. Among all the studied phosphors, the $\text{CaMoO}_4\text{-SO}_4:\text{Sm}^{3+}$ phosphor showed the strongest PL emission compared to all other phosphors suggesting that it is a promising potential candidate for red emission in the near UV excited white LED applications.

Keywords: CaMoO_4 powders, anionic group, White-LED lighting, molybdate

Corresponding authors E-mail addresses: balakrishna.veera@gmail.com, swarthc@ufs.ac.za and ntwaeab@gmail.com

1. Introduction:

Today, light-emitting diodes (LEDs) are widely used in solid state lighting thereby generating research interest in the development of advanced materials that can serve as source of light in LED applications. Since the realization of GaN or near-ultraviolet (NUV) based light-emitting diode (LED), solid-state lighting emission based on phosphor converted (pc) white LEDs have generated interest because of their great advantages over the conventional incandescent and fluorescent lamps [1–6]. The general approach of producing white light is by combining a blue LED chip with a yellow color emitting phosphor (YAG:Ce³⁺). However, this combination has a low color rendering index factor (CRI) because of the poor red component in the YAG:Ce³⁺ phosphor. The combination of a NUV LED with red, green and blue color emitting phosphors is another alternative that may provide a high CRI factor [7]. Therefore, the development of new red-emitting phosphors that can be excited by a near ultraviolet (NUV) (350–420 nm) LED is necessary. Rare earth ions (RE³⁺) doped molybdate phosphors have been evaluated extensively and they have made significant advances in white LEDs [8–11]. Among the rare-earth ions, the Sm³⁺(4f⁵) ion is one of the most promising sources of red light. The red emission associated with the ⁴G_{5/2}→⁶H_{9/2} transition of Sm³⁺ exhibits a relatively high quantum efficiency. In addition, the Sm³⁺ ions exhibit different quenching emission channels defined from the features of the excited state relaxation dynamics of the luminescence in the host materials [12,13]. Compared to other available rare earth dopants, Sm³⁺ ions are very popular because of its reddish orange emission in the visible region. Sm³⁺ ions belongs to the 4f⁵ configuration and in any crystal field perturbation it is doubly generated. The excitation spectra of Sm³⁺ ions doped materials covers the UV, blue and bluish-green spectral range Therefore it is possible to get the reddish orange emission by excitation in this region. The emission profile of Sm³⁺ ions is narrow and it shows longer life times, similar to Eu³⁺ ions. Sm³⁺ ions doped materials are, however, a better alternative. The reddish-orange fluorescence from the Sm³⁺ ions is aligned to the emission peak of the NUV-emitting InGaN chips. Today, the development of Sm³⁺ doped phosphors for NUV LEDs such as NaGd(WO₄)₂:Sm³⁺[14], Ba₂CaWO₆:Sm³⁺[15], Ba₃La(PO₄)₃:Sm³⁺ [16] and La₂WMo₂O₉:Sm³⁺[17] has been reported. Molybdates are being considered as attractive host materials due to their chemical and thermal stability and excellent luminescent properties, among other things. Recently, Sm³⁺-doped molybdates, such as CaLa(MoO₄)₂:Sm³⁺ [18], CdMoO₄:Sm³⁺ [19] and LaMoBO₆:Sm³⁺ [20] have been investigated extensively as potential red-emitting

phosphors for NUV GaN chip-based W-LEDs. In addition, alkaline-earth metal molybdates have important applications in various fields that involve optical fibers, scintillator materials, catalysis, lithium ion batteries, sensors, detectors, light emitting devices and microwave systems devices [21–25]. For luminescent application, CaMoO_4 is an excellent material due to ease of energy transfer (ET) from the MoO_4 absorption band to the excited states of the luminescent centres (lanthanide-ions) [26,27].

Calcium molybdate CaMoO_4 is a typical scheelite compound and has a tetragonal symmetry with space group $I41/a$ [28–30]. In general, it is an excellent host lattice as it can be excited via the O/Mo ligand-to-metal charge transfer (LMCT). CaMoO_4 has been doped with different rare-earths ions such as Tb^{3+} , Sm^{3+} and Eu^{3+} resulting in phosphors that emit green, orange and red light respectively [31,32]. Up to now, there are only a few reports on the Sm^{3+} doped CaMoO_4 phosphor [33–35] and their luminescence properties are not good-enough for LEDs application. Therefore, some efforts are necessary to improve the luminescence intensity of Sm^{3+} doped molybdate based phosphors. Xi and co-workers synthesized $\text{Na}_5\text{Eu}(\text{MoO}_4)_{4-x}(\text{PO}_4)_x$ ($x \leq 0.10$) phosphors by solid-state reaction and observed the PL emission intensity from $\text{Na}_5\text{Eu}(\text{MoO}_4)_{3.96}(\text{PO}_4)_{0.04}$ that was 5.0 times higher than that of commercial $\text{Y}_2\text{O}_2\text{S}:\text{Eu}^{3+}$ phosphor [36]. In a study conducted by Zhang et al, an improvement in the red PL emission intensity of $\text{NaEu}(\text{MoO}_4)_2$ and anionic (SO_4^{2-} and SiO_3^{2-})-doped $\text{NaEu}(\text{MoO}_4)_2$ was observed [37]. Furthermore, the crystal sites of MoO_4^{2-} ions in improved red photoluminescence was observed from $\text{NaLa}(\text{MoO}_4)_2:\text{Eu}^{3+}$ due to incorporation of SO_4^{2-} or BO_3^{3-} anions [38]. We therefore, substituted different anionic groups into the MoO_4^{2-} sites to improve the emission intensity of the $\text{CaMoO}_4:\text{Sm}^{3+}$.

In this study, $\text{CaMoO}_4:\text{Sm}^{3+}$, $\text{CaMoO}_4\text{-BO}_3:\text{Sm}^{3+}$, $\text{CaMoO}_4\text{-PO}_4:\text{Sm}^{3+}$ and $\text{CaMoO}_4\text{-SO}_4:\text{Sm}^{3+}$ phosphors were prepared by the conventional solid state reaction method. The effects of (BO_3^{3-} , PO_4^{3-} and SO_4^{2-}) substitution on the PL properties of $\text{CaMoO}_4:\text{Sm}^{3+}$ phosphors and the possible mechanism for the PL intensity enhancement are discussed in detail.

2. Experimental

2.1 Sample preparation

$\text{CaMoO}_4:\text{Sm}^{3+}$, $\text{CaMoO}_4\text{-BO}_3:\text{Sm}^{3+}$, $\text{CaMoO}_4\text{-PO}_4:\text{Sm}^{3+}$ and $\text{CaMoO}_4\text{-SO}_4:\text{Sm}^{3+}$ phosphors were synthesized using the solid state reaction method. Highly pure CaCO_3 (99.9%), MoO_3 (99.9%), H_3BO_3 , $\text{NH}_4\text{H}_2\text{PO}_4$ (99.9%), $(\text{NH}_4)_2\text{SO}_4$ and Sm_2O_3 (99.99%) supplied by Sigma–Aldrich in Germany were used as starting materials. The doping concentration of the Sm^{3+} amount in the CaMoO_4 was 1.0 mol%, the same concentration that Zang et al. [33] found as the optimal concentration to obtain the maximum PL intensity. Stoichiometric amounts of all these starting materials were used. The anionic substitution amounts added were, 0.1 mol (0.21 g) H_3BO_3 , 0.1 mol (0.37 g) $\text{NH}_4\text{H}_2\text{PO}_4$, 0.1 mol (0.43 g) $(\text{NH}_4)_2\text{SO}_4$, and 0.01 mol (0.057 g) Sm_2O_3 . All these were mixed thoroughly with few drops of acetone in an agate mortar and dried in an oven for 2 h at 120°C . The dried powders were calcined at 1050°C for 5 h and then cooled at room temperature. Finally, the products were ground gently and were ready for characterization.

2.2 Sample characterization

The XRD patterns were recorded with a Bruker AXS D8 Advance X-ray diffractometer using a nickel-filtered CuK_α radiation ($\lambda = 0.154056$ nm). The particle morphology study was carried out using a JEOL JSM-7800F field emission scanning electron microscope (FE-SEM) coupled with an Oxford X-Max80 energy-dispersive X-ray spectroscopy (EDS) system for chemical composition analysis. Fourier transform infrared (FT-IR) spectra were recorded with a Nicolet 6700 spectrometer in the spectral range of 4000 to 500 cm^{-1} . The UV–vis diffuse reflection spectra were recorded using a Perkin Elmer Lambda 950 UV–vis at room temperature in the range of 300–1800 nm. The PL excitation and emission spectra, and the decay curves were measured with the excitation and emission optical slits set at 0.9 nm using a Edinburgh Instruments FLS980 Fluorescence Spectrometer equipped with a xenon lamp as excitation source. For the lifetime measurements the gate time was fixed at 0.05 ms and the delay time was varied starting from 0.1 ms. All the PL and lifetime measurements were performed in air at room temperature.

3. Results and discussion

3.1 Structural characterization and XRD analysis

In order to obtain detailed crystallographic structural information of the synthesized different $\text{CaMoO}_4:\text{Sm}^{3+}$ phosphors substituted with anionic groups (BO_3^{-3} , PO_4^{-3} and SO_4^{-2}), the Rietveld structure refinements of the $\text{CaMoO}_4:\text{Sm}^{3+}$ phosphors were performed using the Fullprof software program [39] and the results are presented in **Fig. 1**. The observed and calculated intensities, the Bragg reflection positions as well as the difference in intensities between observed and calculated data are shown. While employing the refinement procedure, the Pseudo-Voigt function was used to define the profile shape and a 6 coefficient polynomial function was used as background. A good agreement was observed between the experimental and calculated XRD patterns obtained for the four CaMoO_4 powders as shown in **Fig. 1**.

The refined structural parameters are presented in **Table 1**. The CaMoO_4 host phosphors crystallized in a tetragonal structure with space group I 41/a (88) and lattice constants of $a = b = 5.22 \text{ \AA}$, $c = 11.42 \text{ \AA}$ and cell volume, $V = 311.44 \text{ \AA}^3$. The unit cell polyhedral crystal structure diagram of the CaMoO_4 host material is presented in **Fig. 2**. It consists of Ca^{2+} and MoO_4^{2-} ionic sites which can be easily occupied by Sm^{3+} and different anionic groups (BO_3^{-3} , PO_4^{-3} and SO_4^{-2}). The incorporation of Sm^{3+} ion with anionic groups into the host CaMoO_4 phosphors slightly increased the lattice parameter as follows: $a = b = 5.23 \text{ \AA}$, $c = 11.44 \text{ \AA}$ and $V = 312.25 \text{ \AA}^3$. This change in volume signifies the incorporation of the borate group (BO_3^{3-}) and Sm^{3+} ion into the tetragonal CaMoO_4 host material. Upon substitution of Sm^{3+} and BO_3^{3-} group on Ca^{2+} and MoO_4^{2-} sites, some changes in luminescence characteristics of the incorporated activators are expected. The unit cell of the periodic structure of the CaMoO_4 crystal structure includes the CaO_8 polyhedra and MoO_4 tetrahedral as building blocks. The four existing edges of the CaO_8 polyhedral are shared with another four CaO_8 polyhedral. Each oxygen atom of the CaO_8 polyhedra is connected to the Mo atom of the MoO_4 tetrahedra. Thus the oxygen atom is coordinated with two Ca atoms and one Mo atom within one unit cell. A cubic close packing of CaO_8 polyhedra and MoO_4 tetrahedral units disposed in an ordered manner can explain the scheelite structure molybdates, where the point symmetry can significantly be reduced to S_4 [40-44]. Furthermore, all calcium atoms have eight-fold oxygen coordination, thereby forming distorted deltahedral type [CaO_8] clusters with twelve faces [45].

During the refinement process, the occupancy parameters of the atoms (Ca, Mo and O) comprising the host were evaluated with reference to their insignificant stoichiometric

composition range. **Table 2** presents the Rietveld refined structural parameters of different $\text{CaMoO}_4:\text{Sm}^{3+}$ powder substituted with different anionic group systems.

Fig. 1: Reitveld analysis of different CaMoO_4 phosphors substituted with anionic group systems (BO_3^{-3} , PO_4^{-3} and SO_4^{-2}).

Crystal parameters	Host	CaMoO ₄ :Sm ³⁺ sample			
		CaMoO ₄ :Sm	CaMoO ₄ -BO ₃	CaMoO ₄ -PO ₄	CaMoO ₄ -SO ₄
formulae	CaMoO ₄	CaMoO ₄ :Sm	CaMoO ₄ -BO ₃	CaMoO ₄ -PO ₄	CaMoO ₄ -SO ₄
Formulae weight	800.07	804.4832	774.18	846.3091	774.18
Crystal system	Tetragonal	Tetragonal	Tetragonal	Tetragonal	Tetragonal
Unit Cell parameters	a=b=5.220284, c=11.42849	a=b=5.22531, c=11.43613	a=b=5.23077, c=11.44397	a=b=5.22675, c=11.44088	a=b=5.22725, c=11.43375
Volume	311.442	312.250	313.117	311.553	312.417
Density g/cm ³	4.266	4.322	4.1270	4.1780	4.182

Table1. Crystallographic data for CaMoO_4 samples

Fig. 2: Unit cell sheelite tetragonal structure of the CaMoO_4 crystal-partial substitution of different anionic groupic systems (BO_3^{-3} , PO_4^{-3} and SO_4^{-2}).

Sample	Atom	x	y	z	Occupancy	B	Site
CaMoO ₄	Ca	0.00000	0.25000	0.62500	1.000	0.37	4b
	Mo	0.00000	0.25000	0.12500	1.000	0.41	4a
	O	0.14970	0.00330	0.20980	1.000	0.20	16f
CaMoO ₄ -Sm	Ca	0.00000	0.25000	0.62500	0.990	0.13	4b
	Mo	0.00000	0.25000	0.12500	1.000	0.00	4a
	Sm	0.00000	0.25000	0.62500	0.010	0.13	4b
	O	0.14970	0.00330	0.20980	1.000	0.00	16f
CaMoO ₄ -BO ₃ :Sm	Ca	0.00000	0.25000	0.62500	0.980	0.28	4b
	Mo	0.00000	0.25000	0.12500	0.890	0.00	4a
	Sm	0.00000	0.25000	0.62500	0.020	0.04	4b
	B	0.00000	0.25000	0.12500	0.110	0.00	4a
	O	0.15630	-0.00790	0.21410	1.000	0.00	16f
CaMoO ₄ -PO ₄ :Sm	Ca	0.00000	0.25000	0.62500	0.940	0.50	4b
	Mo	0.00000	0.25000	0.12500	0.974	0.50	4a
	Sm	0.00000	0.25000	0.62500	0.060	0.50	4b
	P	0.00000	0.25000	0.25000	0.113	0.50	8e
	O	0.15420	-0.00930	0.21290	1.000	0.00	16f
CaMoO ₄ -SO ₄ :Sm	Ca	0.00000	0.25000	0.62500	0.990	0.50	4b
	Mo	0.00000	0.25000	0.12500	0.890	0.50	4a
	Sm	0.00000	0.25000	0.62500	0.010	0.50	4b
	S	0.00000	0.25000	0.12500	0.100	0.50	4a
	O	0.14480	-0.00660	0.21160	1.000	0.50	16f

Table 2. Refined structural parameters of four different anionic group systems substituted.

Fig. 3 shows the XRD patterns of CaMoO₄:Sm³⁺, CaMoO₄-BO₃:Sm³⁺, CaMoO₄-PO₄:Sm³⁺ and CaMoO₄-SO₄:Sm³⁺ phosphors. The patterns exhibit all diffraction angles (2θ) of CaMoO₄ observed at 18.8°, 28.9°, 31.4°, 34.4°, 39.5°, 45.7°, 47.2°, 49.4°, 54.2°, 56.3°, 58.1°, 59.6°,

64.9°, 69.3°, 72.3° and 76.2°. These peaks correspond to the (101), (112), (004), (200), (211&114), (213), (204), (220), (116), (215), (312), (224), (321), (323), (400) and (316) planes, which can be indexed to the pure scheelite-type tetragonal structure with a space group of I41/a, referenced in international tables of crystallography (No. 88), and point-group symmetry C_{4h}^6 [46-50] of CaMoO_4 . As shown in **Fig. 3**, the XRD patterns are indexed to the standard CaMoO_4 (JCPDS 29-0351) phase, which reveal that the phosphors exhibited identical structures. The uniform diffraction pattern means that phase formation of CaMoO_4 was not influenced by small amounts of Sm^{3+} dopant ion and BO_3^{-3} , PO_4^{-3} and SO_4^{-2} anions. The substitution of Sm^{3+} into Ca^{2+} sites is highly probable due to similarities between the ionic radii of the Sm^{3+} (0.0964 nm, eight-coordinated) and Ca^{2+} ($r=0.112$ nm), which resulted in the formation of an eight coordination with nearby oxygen atoms. Consequently, the crystal structure did not change significantly.

It is interesting to note that the diffraction peaks of the $\text{CaMoO}_4\text{-BO}_3\text{:Sm}^{3+}$, $\text{CaMoO}_4\text{-PO}_4\text{:Sm}^{3+}$ and $\text{CaMoO}_4\text{-SO}_4\text{:Sm}^{3+}$ were less intense relative to those of $\text{CaMoO}_4\text{:Sm}^{3+}$. Some small changes can be observed in the enlarged version of the XRD spectra in **Fig. 4**. It shows that with the substitution of BO_3^{-3} , PO_4^{-3} and SO_4^{-2} anions, the diffraction peaks shifted to higher 2θ values. These shifts were assigned to strains due the fact that the ionic radius of B^{3+} (41 pm), P^{5+} (52 pm) and S^{6+} (43 pm) is smaller than that of Mo^{6+} (73 pm) [51, 52].

Fig. 3: XRD patterns of $\text{CaMoO}_4\text{:Sm}^{3+}$, $\text{CaMoO}_4\text{-BO}_3\text{:Sm}^{3+}$, $\text{CaMoO}_4\text{-PO}_4\text{:Sm}^{3+}$ and $\text{CaMoO}_4\text{-SO}_4\text{:Sm}^{3+}$ phosphors.

Fig. 4: Enlarged version of 101 and 112 diffraction peaks in the XRD patterns of $\text{CaMoO}_4\text{:Sm}^{3+}$, $\text{CaMoO}_4\text{-BO}_3\text{:Sm}^{3+}$, $\text{CaMoO}_4\text{-PO}_4\text{:Sm}^{3+}$ and $\text{CaMoO}_4\text{-SO}_4\text{:Sm}^{3+}$ phosphors.

It also can be seen that the phases of the anionic groups were not detected in the $\text{CaMoO}_4\text{:Sm}^{3+}$, which may be due to the fact that borates, phosphates and sulphates are amorphous [53, 54]. These results demonstrate that highly crystallized Sm^{3+} - doped CaMoO_4 phosphors with SO_4^{2-} , PO_4^{3-} and BO_3^{3-} substitution could be obtained using a simple solid state reaction.

The line broadening of the high intensity diffraction peaks was used to calculate the average crystallite size (d) of the phosphors using Scherrer's formula [55]. The average crystallite sizes of different $\text{CaMoO}_4:\text{Sm}^{3+}$, $\text{CaMoO}_4\text{-BO}_3:\text{Sm}^{3+}$, $\text{CaMoO}_4\text{-PO}_4:\text{Sm}^{3+}$ and $\text{CaMoO}_4\text{-SO}_4:\text{Sm}^{3+}$ phosphors were calculated by Scherrer's formula and were found to be ~52, 70, 41 and 44 nm, respectively. For further confirmation of the crystallite sizes, the Williamson–Hall (W–H) equation was also used. The shape induced strain and crystallite size were estimated from the XRD patterns by using W-H method. Calculations were made using the full width at half maximum (FWHM) of the diffraction peaks and the W-H equation [56,57]. The plots of $\beta_{FWHM}\cos\theta/\lambda$ as a function of $\sin\theta/\lambda$ of the four different samples are shown in **Fig. 5**. The crystallite sizes and the strains were estimated from the best fitted line. From the figure, the crystallite sizes were estimated from the y-intercept and the strains were estimated from the slope. A comparison of the crystallite size and strain values is presented in **Table 3**.

Sample	Average crystal size (nm)		Strain (10^{-3})
	Scherrer	W-H plots	
$\text{CaMoO}_4:\text{Sm}^{3+}$	52	77	1.6
$\text{CaMoO}_4\text{-BO}_3:\text{Sm}^{3+}$	70	72	1.0
$\text{CaMoO}_4\text{-PO}_4:\text{Sm}^{3+}$	41	50	0.74
$\text{CaMoO}_4\text{-SO}_4:\text{Sm}^{3+}$	44	58	0.84

Table 3: Estimated crystallite size and strain values of different $\text{CaMoO}_4:\text{Sm}^{3+}$ phosphor using Scherrer's equation and W-H plot.

The calculated crystallite size values fall in the nanometer range. The strain and size values do not follow a similar trend for all the different anionic group substitution. In general, the strain is reduced in the case of the bigger particles. The difference in crystallite sizes resulted in non-uniform strain values, as listed in **Table 3**. The effective shape induced strain decreased for the co-doped $\text{CaMoO}_4:\text{Sm}^{3+}$ phosphors and were found to be higher in the $\text{CaMoO}_4\text{-BO}_3:\text{Sm}^{3+}$ phosphors because of the nearest ionic radii of B^{3+} (96 pm) to that of Sm^{3+} when compared to the other anions. The crystallite sizes estimated from the W–H plots were to some extent higher than

those determined using Scherrer's method. The inconsistency in the values was due to the fact that in Scherrer's method, the strain component was assumed to be zero and the broadening of XRD of the diffraction peak due to the instrument was neglected.⁵⁸ Usually, prepared samples by solid-state reaction based samples produces various sizes of particles, leading to non-uniform strain within the crystal.

Fig 5: W-H plots of the four different $\text{CaMoO}_4:\text{Sm}^{3+}$ phosphors.

3.3. Surface characterization by X-ray photoelectron spectroscopy (XPS)

The chemical composition and the valance states of the samples were examined by XPS. The typical XPS full survey spectra in Fig. 6 (a)-(d) show the chemical composition of the $\text{CaMoO}_4:\text{Sm}^{3+}$ (1 mol %) phosphors substituted with different anionic groups (BO_3^{-3} , PO_4^{-3} and SO_4^{-2}), and they confirm that all the chemical elements were present as identified by the Ca 2p, Mo 3d, O 1s, C 1s, B 1s, P 2p, S 2p and Sm 3d peaks present in our materials.

Fig. 6: XPS survey scan spectra of different $\text{CaMoO}_4:\text{Sm}^{3+}$ phosphors substituted with different anionic groups.

Fig. 7(a)-(d) show the core level XPS spectra of Ca 2p, Mo 3d, O 1s, C 1s in $\text{CaMoO}_4\text{-SO}_4:\text{Sm}^{3+}$ phosphors. Fig. 7(a) shows the XPS peak of $\text{CaMoO}_4\text{-SO}_4:\text{Sm}^{3+}$ phosphors corresponding to Ca (2p) with a core binding energy (BE) of 345.3 eV for $2p_{3/2}$ and 348.9 eV for $2p_{1/2}$ [59]. These results confirm the presence of the +2 oxidation state of Ca in the $\text{CaMoO}_4\text{-SO}_4:\text{Sm}^{3+}$ phosphors. The Mo 3d spectrum of $\text{CaMoO}_4\text{-SO}_4:\text{Sm}^{3+}$ phosphors are shown in Fig. 7 (b). The XPS peaks corresponding to the Mo (3d) in the phosphor with a core BE of 230.7 eV for the $3d_{5/2}$ and 233.8 eV for the $3d_{3/2}$ with the FWHM of 1.51 and 1.68 eV respectively. These were identified as Mo^{6+} [60]. The C 1s curve in Fig. 7 (c) shows a strong peak at 282.5 eV, shown which is assigned to the aliphatic C–C chain. This is consistent with the residual carbon and the carbon concomitant in the vacuum chamber. Fig. 7(d) shows the O1s core-level spectrum, and three Gaussians were resolved by a curve-fitting procedure. The peak at the lower energy of 528.8 eV is in agreement with that for O^{2-} in CaMoO_4 . The higher energy XPS peak of O 1s for the $\text{CaMoO}_4\text{-SO}_4:\text{Sm}^{3+}$ phosphors is located at 530.0 eV, which is attributed to oxygen

bonding of the SO_4^{2-} network [61]. Based on the above considerations, it is found that valences of Mo(VI) and O(II) elements is +2, further confirming the valence of Ca and S element in $\text{CaMoO}_4\text{-SO}_4\text{:Sm}^{3+}$ is +2 and +6. Additionally, the high energy side of the O(1s) peak is due to hydroxyl groups $-\text{OH}$ or other radicals on the sample surface, such as CO or CO_2 [62]. However, the asymmetric behavior of the high energy peak (~ 530.0 eV) in an O 1s spectrum indicates the presence of oxygen ion vacancies in the lattice [63].

Fig. 7. The high resolution XPS scan spectra of (a) Ca 1s (b) Mo 3d (c) C 1s and (d) O 1s for the $\text{CaMoO}_4\text{-SO}_4\text{:Sm}^{3+}$ phosphors. Gaussian fit of O 1s is shown in (d).

Fig. 8(a) shows the high-resolution XPS spectra of B 1s of $\text{CaMoO}_4\text{-BO}_3\text{:Sm}^{3+}$ phosphor. The spectra are deconvoluted into two Gaussian peaks located at 190.3 and 191.0 eV, indicating the formation of an additional B containing compound. The higher binding energy component 191.0 eV is attributed to the formation of B_2O_3 , which does not normally contribute to the activity of the sample [64-66]. The lower binding energy component at 190.0 eV is due to boron entering the oxygen vacancy substitutionally, which has been reported to be responsible for the origin of visible light [67, 68]. The P 2p XPS peak is located at 131.6 eV in the spectrum shown in Fig. 8 (b), suggesting that phosphorus was stable in the form of pentavalent oxidation state (P^{5+}) [69]. Since the bonding energy of P–O (502 kJ/mol) is stronger than that of Ca–O (486.8 kJ/mol), PO_4^{3-} group is difficult to break compared to Ca–O in the $\text{CaMoO}_4\text{-PO}_4\text{:Sm}^{3+}$ phosphor. Therefore, the existence of PO_4^{3-} group on the surface of CaMoO_4 sample cannot be excluded. Fig. 8(c) shows the XPS spectrum of S 2p. The two weak peaks appearing at the binding energies of 161.3 and 164.5 eV are ascribed to the S $2p_{3/2}$ and S $2p_{1/2}$ of the S^{2-} chemical state, respectively. Based on the literature, [70] the peak at the binding energy of 164.5 eV is assigned to the sulfur in the S^{6+} chemical state on the substituted compound, as in NH_4SO_4 [70]. The binding energies of SO_3 and SO_4 were located at 169.9 eV and 171.4 eV respectively, providing evidence for the existence of S (VI) oxides in the S 2p photoelectron spectra as shown in Fig. 8(c).

Fig. 8: The high resolution XPS spectra of (a) B 1s (b) P 2s and (c) S 2p.

Fig. 9 shows the Sm 3d core level spectra for the Sm doped samples. The two chemical states of Sm^{3+} in the present samples, namely $3d_{5/2}$ and $3d_{3/2}$ are located at 1081.1 eV and 1108.0 eV respectively. These peaks were identical in all four $\text{CaMoO}_4:\text{Sm}^{3+}$ phosphors. Hence, in all four $\text{CaMoO}_4:\text{Sm}^{3+}$ phosphor powders, the Sm exists in a 3+ valance state. According to previous report, Sm^{3+} exist in the powder composites as network modifier instead of network former because of its large ionic radius and high coordination number [71, 72]. Sm^{3+} has the largest radius among all the cations except Ca^{2+} in this system, so the Sm^{3+} is too large to replace other cations. When Sm^{3+} enters the lattice, it can only replace Ca^{2+} sites because of their similar ionic radii [73].

Fig. 9: High resolution XPS Sm 3d spectrum.

3.2 Particle morphology of $\text{CaMoO}_4:\text{Sm}^{3+}$

Fig. 10 (a), (b), (c) and (d) show the SEM images of all the samples. The images indicate that the particles were agglomerated together with well-defined grain boundaries. With addition of anionic groups (BO_3^{3-} , PO_4^{3-} and SO_4^{2-}), the particle sizes became bigger for PO_4^{3-} and BO_3^{3-} and they became smaller in the case of SO_4^{2-} . The reason for the discrepancy in the particle size induced by anionic substitution is not known yet. The related EDS spectra presented in **Fig. 10 (a), (b), (c) and (d)** confirm the presence of all the elements present in our materials with actual mole ratios approaching the stoichiometric values as shown in the inset.

Fig. 10 (a), (b), (c) and (d): The SEM images and EDS spectra of different $\text{CaMoO}_4:\text{Sm}^{3+}$ phosphors substituted with anionic groups.

3.3. FT-IR study

Fig. 11 shows the FT-IR spectra of different $\text{CaMoO}_4:\text{Sm}^{3+}$ phosphors substituted with anionic groups (BO_3^{3-} , PO_4^{3-} and SO_4^{2-}). The spectra of all $\text{CaMoO}_4:\text{Sm}^{3+}$ samples are similar, except for strong absorption peaks appearing around at 1120 cm^{-1} are assigned to BO_3^{3-} , PO_4^{3-} and SO_4^{2-} vibrations and they are present in the $\text{CaMoO}_4\text{-BO}_3:\text{Sm}^{3+}$, $\text{CaMoO}_4\text{-PO}_4:\text{Sm}^{3+}$ and

CaMoO₄-SO₄:Sm³⁺ phosphors, respectively. In addition, the spectra further confirm that anion groups (SO₄²⁻, PO₄³⁻ and BO₃³⁻) were present in CaMoO₄-BO₃:Sm³⁺, CaMoO₄-PO₄:Sm³⁺ and CaMoO₄-SO₄:Sm³⁺ phosphors and this is in agreement with the XRD results. Different prominent bands were detected around 424, 811, 1063 and 1217 cm⁻¹. A strong absorption band at 811 cm⁻¹ is related to the O–Mo–O stretching frequency mode and that at 424 cm⁻¹ is attributed to the stretching vibration of Mo–O [74,75]. For Sm³⁺ doped samples, similar peaks were observed. No significant change in the peak position was observed from the un-doped and anionic groups doped samples. This is because the lanthanide ions were most likely doped in the lattice site of the CaMoO₄ host and hence their FT-IR spectra show similar peaks to that of the host.

Fig. 11: The FT-IR spectra of different CaMoO₄:Sm³⁺ phosphors substituted with anionic groups.

3.4 Ultraviolet–visible absorption spectroscopy:

The diffuse reflectance spectra (DRS) measured in the spectral region of 300-1800 nm are shown in **Fig. 12**. The peak at 306 nm from all the spectra is attributed to charge transfer from oxygen (2p) ligand to the central molybdenum (Mo) atom in MoO₄²⁻ ion [76-78]. This is similar to previous observations reported in refs. [79-81]. The absorption peak around at 1245 nm is ascribed to the (⁶H_{5/2}→⁶F_{7/2}) transition of Sm³⁺ [82]. In all the DRS spectra, several optical bands were observed in the region above 400 nm and each band originates from the characteristic transitions of the Sm³⁺ ion, which are attributed to the transitions between the ⁶H_{5/2} ground state and different excited states such as ⁶P_{3/2}, ⁴I_{9/2}+⁴M_{15/2}+⁴I_{13/2}, ⁶F_{11/2}, ⁶F_{9/2}, ⁶F_{7/2}, ⁶F_{5/2}, ⁶F_{3/2}, ⁶F_{1/2} and ⁶H_{15/2} of Sm³⁺. In the case of CaMoO₄-SO₄:Sm³⁺ phosphors in the UV-vis region, the optical absorption was noticed at higher wavelength compare to the other studied phosphors. The strong absorption band from 300 to 340 nm could be attributed to the absorption of the host materials, suggesting that CaMoO₄:Sm³⁺ phosphors can be excited by n-UV LEDs. It is worth noting that in the diffuse reflectance spectra of Sm³⁺-doped CaMoO₄-SO₄, the full width at half-maximums (FWHMs) of the absorption bands of Sm³⁺ ions are very strong, compared to other Sm³⁺-doped hosts such as Ba₃Bi(PO₄)₃, Sr₃2xSm_xNa_xB₂SiO₈ and Na₆CaP₂O₉ [80-82].

When the different anionic groups (BO_3^{3-} , PO_4^{3-} and SO_4^{2-}) were substituted into the $\text{CaMoO}_4:\text{Sm}^{3+}$ phosphors, several weak absorption bands were enhanced in the larger wavelength range of 920–1670 nm (i.e., towards low energy). Especially for the absorption bands originating from the ${}^6\text{H}_{5/2} \rightarrow ({}^6\text{F}_{3/2}, {}^6\text{F}_{1/2}, {}^6\text{H}_{15/2})$ transitions, the FWHMs of absorption bands were widened and the Stark components became complicated. One possible reason for this observation is that in the $\text{CaMoO}_4:\text{Sm}^{3+}$ systems there are three nonequivalent crystal lattice sites to which Mo^{6+} are 4-fold coordinated, while Ca^{2+} and Sm^{3+} ions are 8-fold coordinated. The Sm^{3+} ions occupying the Ca^{2+} sites can reside in more than one crystallographic sites, therefore the absorption lines of Sm^{3+} ions became more intense and wider, which can be attributed to the substitution of larger sized MoO_4^{2-} sites by the smaller sized SO_4^{2-} , PO_4^{3-} and BO_3^{3-} in $\text{CaMoO}_4:\text{Sm}^{3+}$ and this has also been observed in different rare earths doped hosts [83-85]. The wider FWHMs of absorption bands of Sm^{3+} in $\text{CaMoO}_4\text{-SO}_4:\text{Sm}^{3+}$ are helpful to allow the excitation wavelength shift of blue LED chips.

Fig. 12: The diffuse reflectance spectra (DRS) measured of the different $\text{CaMoO}_4:\text{Sm}^{3+}$ phosphors in the spectral region of 300-1800 nm.

The diffuse reflectance data were used to estimate the optical band gap (E_G) values using the Kubelka Munk (K–M) function [83,85]. Particularly, it can be used in limited cases of infinitely thick sample layer. Based on this position, the optical band gap energy (E_G) can be evaluated from the data presented in **Fig. 13**. The steep absorption edges in the range of 3.0–3.4 eV for the four different $\text{CaMoO}_4:\text{Sm}^{3+}$ phosphors are due to the intrinsic transition of the host lattice rather than the electronic transitions between the f-f levels of the Sm^{3+} ion [86]. The absorption band energies calculated from the DR spectra using the K–M function $F(R_\infty)$ for all the $\text{CaMoO}_4\text{-BO}_3:\text{Sm}^{3+}$, $\text{CaMoO}_4\text{-BO}_3:\text{Sm}^{3+}$, $\text{CaMoO}_4\text{-PO}_4:\text{Sm}^{3+}$ and $\text{CaMoO}_4\text{-SO}_4:\text{Sm}^{3+}$ phosphors were found to be 3.353, 3.380, 3.276 and 3.302 eV respectively. Due to the substitution of different anionic groups into the $\text{CaMoO}_4:\text{Sm}^{3+}$, the absorption band tends to shift toward the lower energies. The optical band gap energy (E_g) decreased and the absorption improved. The exponential optical absorption edge and the optical band gap energy were controlled by the structural changes in the host lattice. The decrease in the E_G can be attributed to the existence of local defects and bond deformation [87].

Fig. 13: The absorption edges in the range of 3.0–3.4 eV for the four different $\text{CaMoO}_4:\text{Sm}^{3+}$ phosphors.

3.5. Photoluminescent properties of $\text{CaMoO}_4:\text{Sm}^{3+}$: Effect of BO_3^{3-} , PO_4^{3-} and SO_4^{2-}

Fig. 14 shows the PL excitation (PLE) spectra recorded when monitoring the ${}^4\text{G}_{5/2} \rightarrow {}^6\text{H}_{9/2}$ emission peak of Sm^{3+} ion at 646 nm from the different phosphors. These four $\text{CaMoO}_4:\text{Sm}^{3+}$ phosphors showed a broad PLE band ranging from 200 nm to 500 nm with some narrow peaks centered at 286, 346, 363, 377, 392, 405, 408, 421, 440, 464 and 482 nm. Generally, the wide band is formed by $\text{O}^{2-} \rightarrow \text{Sm}^{3+}$ and $\text{O}^{2-} \rightarrow \text{Mo}^{6+}$ charge-transfer (C-T) band [33]. In the present case, the band is ascribed to charge-transfer (CT) band of $\text{O}^{2-} \rightarrow \text{Mo}^{6+}$ and the narrow peaks belongs to the ${}^6\text{H}_{5/2} \rightarrow {}^4\text{D}_{3/2}$, ${}^6\text{H}_{5/2} \rightarrow {}^4\text{D}_{1/2}$, ${}^6\text{H}_{5/2} \rightarrow {}^6\text{p}_{7/2}$, ${}^6\text{H}_{5/2} \rightarrow {}^6\text{L}_{15/2}$, ${}^6\text{H}_{5/2} \rightarrow {}^4\text{F}_{7/2}$, ${}^6\text{H}_{5/2} \rightarrow {}^4\text{M}_{19/2}$, ${}^6\text{H}_{5/2} \rightarrow {}^4\text{I}_{13/2}$, ${}^6\text{H}_{5/2} \rightarrow {}^4\text{M}_{15/2}$, ${}^6\text{H}_{5/2} \rightarrow {}^4\text{I}_{9/2}$ and ${}^6\text{H}_{5/2} \rightarrow {}^4\text{G}_{7/2}$ characteristic transitions of Sm^{3+} ions. The peak at 404 nm is more intense and it corresponds to the emission wavelength of InGaN based LED chips. Hence the phosphor could be efficiently excited by the near UV LEDs.

Fig. 14: The PL excitation (PLE) spectra recorded when monitoring the ${}^4\text{G}_{5/2} \rightarrow {}^6\text{H}_{9/2}$ emission peak of Sm^{3+} ion at 646 nm for the four different $\text{CaMoO}_4:\text{Sm}^{3+}$ phosphors.

Fig. 15 shows the PL emission (PL) spectra of the different $\text{CaMoO}_4:\text{Sm}^{3+}$ phosphors substituted with SO_4^{2-} , PO_4^{3-} and BO_3^{3-} anionic groups. The spectra were measured when exciting the wavelength of 404 nm. Four emission peaks, namely 563, 605, 646 and 706 nm, with the strongest emission peak located at 646 nm, were observed. The peak at 563 nm is attributed to the ${}^4\text{G}_{5/2} \rightarrow {}^6\text{H}_{5/2}$ transition within the scanning range of 550 to 577 nm; the peak at

605 nm is attributed to the ${}^4G_{5/2} \rightarrow {}^6H_{7/2}$ transition within the scanning range of 580 to 620 nm; the peak at 646 nm is attributed to the ${}^4G_{5/2} \rightarrow {}^6H_{9/2}$ transition within the scanning range of the 625 to 670 nm; and the peak at 706 nm is attributed to the ${}^4G_{5/2} \rightarrow {}^6H_{11/2}$ transition within the scanning range of 685 to 720 nm. All the four emission peaks are attributed to the f→f transitions in the 4f electron shell of Sm^{3+} ion [88, 89]. The shape and peak positions of the $CaMoO_4:Sm^{3+}$ emission spectra did not vary with the substitution of anionic groups, indicating that the different anions substitution did not influence the electronic transition in $CaMoO_4:Sm^{3+}$ phosphor. Furthermore the substitution of anionic groups enhanced the PL intensities. For example, the PL emissions of $CaMoO_4-BO_3:Sm^{3+}$, $CaMoO_4-PO_4:Sm^{3+}$ and $CaMoO_4-SO_4:Sm^{3+}$ are 30 times more intense than that of $CaMoO_4:Sm^{3+}$ phosphors. This indicates that the substitution of different anions into the $CaMoO_4:Sm^{3+}$ enhanced the photoluminescence emission intensity considerably.

Fig. 15: The PL emission spectra of the different $CaMoO_4:Sm^{3+}$ phosphors substituted with SO_4^{-2} , PO_4^{-3} and BO_3^{-3} anionic groups.

This can be explained by the increase in the excitation of the UV light for the $CaMoO_4:Sm^{3+}$ phosphor due to the anion substitution. Therefore, more excitation UV light is easily absorbed by $CaMoO_4:Sm^{3+}$ phosphor due to the presence of different anionic structural phases, resulting in the enhancement of luminescent intensity [36–38]. In the $CaMoO_4:Sm^{3+}$ phosphor, one Sm^{3+} ion is expected to replace one Ca^{2+} ion. If so, it would be difficult to keep charge balance in the phosphor sample. Therefore, Sm^{3+} ions may not be fully introduced into the Ca ion sites in order to keep charge balance. Additionally, some cations may exist in ‘CaO’ defect states instead of forming $CaMoO_4$ with MoO_3 and produce vacancies (V_{Ca}) that act as luminescent quenchers. Both possible mechanisms to maintain chemical neutrality in $CaMoO_4:Sm^{3+}$ phosphor would lead to the less emission intensity, because the impurity phase, Sm_2O_3 and CaO , could restrain the $CaMoO_4$ grain growth during the sintering process. However, in anionic substituted phosphor samples, namely $CaMoO_4-BO_3:Sm^{3+}$, $CaMoO_4-PO_4:Sm^{3+}$ and $CaMoO_4-SO_4:Sm^{3+}$, Sm^{3+} , it is most likely that the ions could easily occupy the Ca^{2+} sites. The anionic substitution did not only enhanced the PL emission intensity it also tuned the emission colour from reddish-orange to red.

3.6. Lifetime study

The kinetic decay curves of the $\text{CaMoO}_4:\text{Sm}^{3+}$ phosphors substituted with different anionic groups were measured for the 646 nm emission excited at 406 nm, and the data are presented in **Fig. 16**. The decay curves were fitted with the bi-exponential function. The bi-exponential behavior is dependent on the number of luminescent centers created by the Sm^{3+} ion dopant, energy transfer from the donor to the activator and defects present in the host [90]. All the PL decay curves were fitted with the following bi-exponential decay equation,

$$I(t) = I_0 + A_f \exp\left(-\frac{t}{\tau_f}\right) + A_s \exp\left(-\frac{t}{\tau_s}\right) \quad (1)$$

where I is the luminescence intensity, where τ_f and τ_s are the fast and slow decay times respectively and A_f and A_s are their respective weight. The lifetime values were obtained for the fast and slow decay phenomena and are listed in Table 4. The average lifetime was determined using [91]:

$$\tau_{avg} = \frac{(A_f \tau_f^2 + A_s \tau_s^2)}{A_f \tau_f + A_s \tau_s} \quad (2)$$

The average lifetime τ_{avg} values were found to be 654, 429, 572 and 490 μs for $\text{CaMoO}_4:\text{Sm}^{3+}$, $\text{CaMoO}_4\text{-BO}_3:\text{Sm}^{3+}$, $\text{CaMoO}_4\text{-PO}_4:\text{Sm}^{3+}$ and $\text{CaMoO}_4\text{-SO}_4:\text{Sm}^{3+}$ respectively. The lifetimes of the luminescent centers are shown to decrease along with the substitution of different anionic groups, which is due to the fact that Sm^{3+} ions substitute into the Ca^{2+} ions for the combined anionic phosphors made the electrons transitions from higher energy states to lower energy states. This could shorten the time the electrons stay in the specific energy level. It is worth noting that the average lifetime (τ) values of the SO_4 and BO_3 substitution of $\text{CaMoO}_4\text{-SO}_4:\text{Sm}^{3+}$ and $\text{CaMoO}_4\text{-BO}_3:\text{Sm}^{3+}$ are much smaller than that of $\text{CaMoO}_4:\text{Sm}^{3+}$ phosphors, indicating the more profound replacement of Sm^{3+} ions into the CaMoO_4 lattice.

Fig. 16: The fluorescence decay curves of Sm^{3+} ion in different $\text{CaMoO}_4:\text{Sm}^{3+}$ phosphors substituted with anionic groups (BO_3^{-3} , PO_4^{-3} and SO_4^{-2}) by monitoring 646 nm from the transitions of ${}^4G_{5/2} \rightarrow {}^6H_{9/2}$ under the excitation of 403 nm.

Sample	Double Exponential fitting factors				Average life time (μs)
	A_f	$\tau_f(\mu\text{s})$	A_s	$\tau_s(\mu\text{s})$	
$\text{CaMoO}_4:\text{Sm}^{3+}$	4640	22	1890	703	654
$\text{CaMoO}_4\text{-BO}_3:\text{Sm}^{3+}$	3602	57	1523	525	429
$\text{CaMoO}_4\text{-PO}_4:\text{Sm}^{3+}$	2780	76	396	585	572
$\text{CaMoO}_4\text{-SO}_4:\text{Sm}^{3+}$	1632	55	3576	511	490

Table 4. Decay times of the luminescence of $^4G_{5/2} \rightarrow ^6H_{9/2}$ transition in different $\text{CaMoO}_4:\text{Sm}^{3+}$ phosphors.

3.7. Color coordinates of phosphors-orange to red color shifting

To evaluate the effect of different anionic group substitution on the luminescent colors, the CIE (Commission International del'Eclairage) chromaticity coordinates of the $\text{CaMoO}_4:\text{Sm}^{3+}$ phosphors were calculated by using the emission spectra and are shown in **Fig. 17**. The CIE chromaticity coordinates of a fluorescence system are very important certification for photoluminescence applications [92]. Every natural color could be identified by (x,y) coordinates that are determined using CIE chromaticity diagram. As shown in **Fig 17**, the color coordinates of $\text{CaMoO}_4:\text{Sm}^{3+}$ and $\text{CaMoO}_4\text{-BO}_3:\text{Sm}^{3+}$, $\text{CaMoO}_4\text{-PO}_4:\text{Sm}^{3+}$ and $\text{CaMoO}_4\text{-SO}_4:\text{Sm}^{3+}$ phosphors are all in the red region. All phosphors have a similar value, which are quite close to the standard red chromaticity (0.67, 0.33) for the National Television Standard Committee system. In addition, by comparing the CIE values (x, y) among all $\text{CaMoO}_4:\text{Sm}^{3+}$ systems, it can be seen that the CIE values (x, y) shifted significantly from the reddish orange to the red region due to the substitution of the anionic group. This result confirms the role of different anionic substitution into the $\text{CaMoO}_4:\text{Sm}^{3+}$ phosphors. Therefore, the phosphors $\text{CaMoO}_4:\text{Sm}^{3+}$ with different anionic groups may possess great potential for commercial applications. It is seen that the colors of the phosphors shift gradually from the orange (0.571, 0.423) to the red color region (0.627, 0.366) with substitution of the different anionic groups, confirming that their emission colors are tunable. Upon exciting at 408 nm xenon lamp, the same trend from orange to red color

for all $\text{CaMoO}_4\text{-BO}_3\text{:Sm}^{3+}$, $\text{CaMoO}_4\text{-PO}_4\text{:Sm}^{3+}$ and $\text{CaMoO}_4\text{-SO}_4\text{:Sm}^{3+}$ phosphors was observed. Therefore, the orange-red tunable emission of all the studied systems can be realized when the excitation wavelength is located at 403 nm, which is suitable for application in n-UV based WLEDs.

Fig. 17: CIE chromaticity coordinates of the $\text{CaMoO}_4\text{:Sm}^{3+}$ phosphors a) $\text{CaMoO}_4\text{:Sm}^{3+}$ b) $\text{CaMoO}_4\text{-BO}_3\text{:Sm}^{3+}$, c) $\text{CaMoO}_4\text{-PO}_4\text{:Sm}^{3+}$ and d) $\text{CaMoO}_4\text{-SO}_4\text{:Sm}^{3+}$ The insets show the corresponding digital photographs of samples under the excitation of a 404 nm Xenon lamp.

3.8. Photon distribution and quantum yield

The quantum yield of Sm^{3+} emission in the studied phosphor powders were evaluated from the photon distribution $N(\bar{\nu})$. The $N(\bar{\nu})$ spectrum can be deconvoluted into two components: reflected light from the excitation source and fluorescence from the powders as shown in **Fig. 18**. The photon distribution of the source set to 404 nm reflected from Spectralon is shown as curve 1 (red color line). To show the absorption extent of the pumping energy, the photon distribution of excitation source reflected from the sample is also shown as curve 2 (black color line). By subtracting curve 1 from curve 2, the absorbed photon number can be estimated by integrating the distribution with wavelength. The emitted photon number can also be evaluated from integrating the fluorescence component

Fig. 18: Spectral power distribution of Sm^{3+} ion in different $\text{CaMoO}_4\text{:Sm}^{3+}$ phosphors substituted with anionic groups.

The quantum yield QY is defined by:

$$\text{QY} = \frac{\text{emitted photons}}{\text{absorbed photons}}$$

The QY of four different $\text{CaMoO}_4\text{:Sm}^{3+}$ phosphors was calculated to be 0.53, 16, 12 and 21%, respectively. The quantum efficiency of the present Sm^{3+} ion doped CaMoO_4 materials are well comparable and found in some cases higher than that of other Sm^{3+} ion doped glass materials [93, 94].

Conclusion

In summary, a series of novel red emitting, $\text{CaMoO}_4:\text{Sm}^{3+}$ phosphors, substituted with different anionic groups (BO_3^{-3} , PO_4^{-3} and SO_4^{-2}) were successfully synthesized using the high temperature solid state reaction method. Anionic substitution did not affect the crystal structure but it influenced the photoluminescence luminescence intensity and emission colour. The XPS analysis indicated variation in the Ca^{2+} surroundings, Mo-O charge transfer energy and oxygen vacancy distribution after substitution of different anionic groupic systems. These changes modified the optical and the luminescence behavior of the material. The PL intensity was 30 times more intense due to anionic substitution. The PL results reveal that the present phosphor can be effectively excited by near UV LED chips to emit in the red region with improved quantum efficiency. With the introduction of the different anionic groups, the optical band gap energy (E_g) decreased. Simultaneously, the CRI of $\text{CaMoO}_4:\text{Sm}^{3+}$ phosphors, vary with the substitution of different anionic groups (BO_3^{-3} , PO_4^{-3} and SO_4^{-2}) into the $\text{CaMoO}_4:\text{Sm}^{3+}$ phosphors. Based on these experimental results, the $\text{CaMoO}_4:\text{Sm}^{3+}$ phosphors can act as potential color-tunable phosphors. Therefore, the different anionic substituted $\text{CaMoO}_4:\text{Sm}^{3+}$ phosphors are expected to be novel red phosphors that can easily be paired with highly efficient InGaN chips for white LED applications.

Acknowledgements:

The research is supported by the South African Research Chairs Initiative of the Department of Science and Technology and the National Research Foundation of South Africa (84415). The financial assistance from the University of the Free State is highly recognized.

References:

- [1] S. Nakamura, T. Mukai, M. Senoh, J. Appl. Phys., 76 (1994) 8189-8191.
- [2] Z.G. Wei, L.D. Sun, C.S. Liao, C.H. Yan, S.H. Huang, Appl. Phys. Lett., 80 (2002) 1447-1449.
- [3] D.K. Williams, B. Bihari, B.M. Tissue, J.M. McHale, J. Phys. Chem. B, 102(1998) 916-920.
- [4] M. Yu, J. Lin, J. Fang, Chem. Mater., 17 (2005) 1783-1791.
- [5] Z.H. Li, J.H. Zeng, Y.D. Li, Small 3(2007) 438-443.

- [6] N. Hirosaki, R.J. Xie, K. Kimoto, T. Sekiguchi, Y. Yamamoto, T. Suehiro, M. Mitomo, *Appl. Phys. Lett.*, 86 (2005) 211905.
- [7] J.S. Kim, P.E. Jeon, Y.H. Park, J.C. Choi, H.L. Park, G.C. Kim, T.W. Kim, *Appl. Phys. Lett.*, 85 (2004) 3696-3698.
- [8] S. Yan, J. Zhang, X. Zhang, S.Z. Lu, X.G. Ren, Z.G. Nie, X.J. Wang, *J. Phys. Chem. C*, 111(35) (2007) 13256-13260.
- [9] E. Cavilli, E. Bovero, A. Belletti, *J. Phys-Condens. Mat.*, 14 (20) (2002) 5221-5228.
- [10] L. Guan L, W. Wei, C. Liu, *J. Chin. Ceram. Soc.*, 40 (12) (2012) 1744.
- [11] X.J. Zhou, T.H. Zhou, Y.M. Li, Q. Feng, *J. Rare Earths*, 30 (4) (2012) 315-319.
- [12] G. Lakshminarayana, R. Yang, J.R. Qiu, M.G. Brik, G.A. Kumar, I.V. Kityk, *J. Phys. D: Appl. Phys.*, 42 (2009) 015414.
- [13] G. Lakshminarayana, R. Yang, M.F. Mao, J.R. Qiu, I.V. Kityk, *J. Non-Cryst. Solids*, 355(2009) 2668-2673.
- [14] A. Durairajan, D. Balaji, K. Kavi Rasu, S. Moorthy Babu, M.A. Valente, D. Thangaraju, Y. Hayakawa, *J. Lumin.*, 170 (2016) 743-748.
- [15] R. Yu, H. Mi Noh, B.K. Moon, B.C. Choi, J.H. Jeong, H.S. Lee, K. Jang, S.S. Yi, *J. Lumin.*, 152 (2014) 133-137.
- [16] R. Yu, H.M. Noh, B.K. Moon, B.C. Choi, J.H. Jeong, H.S. Lee, K. Jang, S.S. Yi, *J. Lumin.*, 145 (2014) 717-722.
- [17] Y. Deng, S. Yi, J. Huang, W. Zhao, J. Xian, *Physica B*, 433 (2014) 133-137.
- [18] V. Mahalingam, M. Syed GulamAmbia, J. Thirumalai, R. Krishnan, R. Chandramohan, *J Mater Sci: Mater Electron*, 27 (9) (2016) 8884-8890.
- [19] M. Li, W. Ran, Z. Chen, D. Qu, L. Zhang, J. Shi, *J Mater Sci: Mater Electron*, 28 (2017) 2642-2650.
- [20] X.M. Zhang, H.J. Seo, *J. Alloys and Compds.*, 509(2011) 2007-2010.
- [21] V.B. Mikhailik, H. Kraus, G. Miller, M.S. Mykhaylyk, D. Wahl, *J. Appl. Phys.*, 97 (2005) 083523.
- [22] L. Wang, Y. Zhao, Q.Y. Lai, Y.J. Hao, *J. Alloys Compd.*, 495 (2010) 82-87.
- [23] J. Zhang, L. Li, W. Zi, N. Guo, L. Zou, S. Gan, G. Ji, *J. Phys. Chem. Solids*, 75, (2014) 878-887.

- [24] R. Graser, E. Pitt, A. Scharmann, G. Zimmerer, *Phys. Status Solidi B*, 69 (1975) 359-368.
- [25] L.F. Johnson, G.D. Boyd, K. Nassau, R.R. Soden, *Phys. Rev.*, 126 (1962) 1406-1409.
- [26] G.S.R. Raju, E. Pavitra, Y.H. Ko, J.S. Yu, *J. Mater. Chem.*, 22 (2012) 15562-15569.
- [27] A.K. Parchur, R.S. Ningthoujam, S.B. Rai, G.S. Okram, R.A. Singh, M. Tyagi, S.C. Gadkari, R. Tewari, R.K. Vatsa, *Dalton Trans.*, 40(2011) 7595-7601.
- [28] S.S. Hosseinpour-Mashkani, S.S. Hosseinpour-Mashkani, A. Sobhani-Nasab, *J Mater Sci: Mater Electron*, 27(2016) 4351-4355.
- [29] V.V. Bakovets, E.S. Zolotova, O.V. Antonova, I.V. Korol'kova, I. V. Yushina, *Technical Physics*, Pleiades Publishing, Ltd., 2016, Vol. 61, No. 7, 1064–1072.
- [30] V.S. Marques, L.S. Cavalcante, J.C. Sczancoski, A.F.P. Alcatara, M.O. Orlandi, E. Moraes, E. Longo, J.A. Varela, M. Siu Li, M.R.M. C. Santos, *Cryst. Growth Des.*, 10 (11) (2010) 4753-4768.
- [31] Y. Liu, J. Zhang, C. Zhang, J. Jiang, H. Jiang, *J. Phys. Chem. C*, 120 (2016) 2362-2370.
- [32] M. İlhan, M.K.Ekmekçi, A.Demir, H. Demirel, *J. Fluoresc.*, 26 (2016) 1637-1643.
- [33] Z.W. Zhang, X.H. Shen, Y.J. Ren, W.L. Hou, W.G. Zhang, D.J. Wang, *Opt. Laser Technol.*, 56 (2014) 348-353.
- [34] A. Kuzmanoski, V. Pankratov, C. Feldmann, *Solid State Sci.*, 41 (2015) 56-62.
- [35] A.A. Ansari, M. Alam, *J. Lumin.*, 157 (2015) 257-263.
- [36] C. Xi, S. Shi, H. Gong, J. Zhou, *Mater. Sci. Forum*, 654–656 (2010) 2025-2028.
- [37] Y. Zhang, S. Shi, J. Gao, J. Zhou, *J. Nanosci. Nanotechnol.* 10 (2010) 2156.
- [38] W. Zhang, J. Li, Y. Wang, J. Long, K. Qiu, *J. Alloys and Compds.*, 635 (2015) 16-20.
- [39] J. Rodriguez-Carvajal, Fullprof, Institute Laue-Langervin, Grenoble, France, 2006.
- [40] T. Thongtem, S. Kungwankunakorn, B. Kuntalue, A. Phuruangrat, S. Thongtem, *J. Alloy. Compd.*, 506 (2010) 475-481.
- [41] A. Phuruangrat, T. Thongtem, S. Thongtem, *Preparation, J. Alloy. Compd.*, 481 (2009) 568-572.
- [42] S. Dutta, S. Som, A.K. Kunti, Vijay Kumar, S.K. Sharma, H.C. Swart, H.G. Visser, *Acta Mater.*, 124 (2017) 109-119.
- [43] T.T. Basiev, A.A. Sobol, Y.K. Voronko, P.G. Zverev, *Opt. Mater.*, 15 (2000) 205-216.

- [44] M. Bomio, R. Tranquilin, F. Motta, C. Paskocimas, R. Nascimento, L. Gracia, J. Andres, E. Longo, *J. Phys. Chem. C*, 117 (2013) 21382.
- [45] L.S. Cavalcante, V.M. Longo, J.C. Sczancoski, M.A.P. Almeida, A.A. Batista, J.A. Varela, M.O. Orlandi, E. Longo, M.S. Li, *Cryst. Eng. Comm.*, 14 (2012) 853-868.
- [46] S. Dutta, S. Som, A.K. Kunti, S.K. Sharma, Vijay Kumar, H.C. Swart, H.G. Visser, *Nucl. Instrum. Methods Phys. Res. B*, 384 (2016) 76-85.
- [47] V.M. Longo, L.S. Cavalcante, E.C. Paris, J.C. Sczancoski, P.S. Pizani, M.S. Li, J. Andres, E. Longo, J.A. Varela, *J. Phys. Chem. C*, 115 (2011) 5207-5219.
- [48] G.S.R. Raju, E. Pavitra, Y.H. Ko, J.S. Yu, *J. Mater. Chem.*, 22 (2012) 15562-15569.
- [49] V.M. Longo, A.T. de Figueiredo, A.B. Campos, J.W.M. Espinosa, A.C. Hernandez, C.A. Taft, J.R. Sambrano, J.A. Varela, E. Longo, *J. Phys. Chem. A*, 112, (2008) 8920-8928.
- [50] A.K. Parchur, A.I. Prasad, A.A. Ansari, S.B. Rai, R.S. Ningthoujam, *Dalton Trans.*, 41 (2012) 11032-11045.
- [51] E. Oz, S. Altin, S. Demirel, A. Bayri, E. Altin, O. Baglayan, S. Avci, *J. Alloys and Compds.*, 657 (2016) 835-847.
- [52] A. Marckwordt, R. Rajasekharan-Nair, G. Steel, A.R. Kennedy, J. Reglinski, Mark D. Spicer, *Eur. J. Inorg. Chem.*, 2016 (2016) 2552-2555.
- [53] M. Cetinkol, A.P. Wilkinson, P.L. Lee, *J. Solid State Chem.*, 182 (2009) 1304-1311.
- [54] L. Aleksandrov, T. Komatsu, K. Shinozaki, T. Honma, R. Iordanova, *J. Non-Cryst. Solids*, 429 (2015) 171-177.
- [55] R.E. Kroon, *Nanoscience and the Scherrer equation versus the 'Scherrer-Gottingen equation*, *S. Afr. J. Sci.* 2013, 109(5/6), Art. #a0019.
- [56] A. Khorsand Zak, W.H. Abd Majid, M.E. Abrishami, R. Yousefi, *Solid State Sci.*, 13 (2011) 251-256.
- [57] A. Durairajan, D. Thangaraju, S. MoorthyBabu, M.A. Valente, *Mater. Chem. Phys.*, 179 (2016) 295-303.
- [58] B. Umesh, B. Eraiah, H. Nagabhushana, S.C. Sharma, D.V. Sunitha, B.M. Nagabhushana, J.L. Rao, C. Shivakumara, R.P.S. Chakradhar, *Mater. Res. Bull.*, 48 (2013) 180-187.

- [59] S.H. Liao, S.Y. Lu, S.J. Bao, Y.N. Yu, M.Q. Wang, *Anal. Chim. Acta*, 905 (2016) 72-78.
- [60] B.P. Singh, A.K. Parchur, R.S. Ningthoujam, A.A. Ansari, P. Singh, S.B. Rai, *Dalton Trans.*, 43 (12) (2014) 4770-4778.
- [61] Q. Zhang, W. Wang, Z. Zhang, J. Zhang, Y. Bai, N. Tsubaki, Y. Han, Y. Tan, *Catal. Sci. Technol.*, 6 (2016) 7193-7202.
- [62] L. R. Shah, B. Ali, H. Zhu, W. G. Wang, Y. Q. Song, H. W. Zhang, S. I. Shah, J. Q. Xiao, *J. Phys.: Condens. Matter*, 21 (2009) 486004.
- [63] A. K. Parchur, A. I. Prasad, S. B. Rai, R. Tewari, R. K. Sahu, G. S. Okram, R. A. Singh and R. S. Ningthoujam, *AIP Adv.*, 2 (2012) 032119.
- [64] S. In, A. Orlov, R. Berg, F. Garcia, S. Pedrosa-Jiménez, M.S. Tikhov, D.S. Wright, R.M. Lambert, *J. Am. Chem. Soc.*, 129 (2007) 13790–13791.
- [65] W.L. Dai, H.X. Li, Y. Cao, M.H. Qiao, K.N. Fan, J.F. Deng, *Langmuir*, 18 (2002) 9605-9608.
- [66] J. Legrand, A. Taleb, S. Gota, M.J. Guittet, C. Petit, *Langmuir*, 18 (2002) 4131-4137.
- [67] W. Zhao, W.H. Ma, C.C. Chen, J.C. Zhao, Z.G. Shuai, *J. Am. Chem. Soc.*, 126 (2004) 4782-4783.
- [68] Md. Hussain Basha, Neeruganti O. Gopal, Dipak B. Nimbalkar, Shyue-Chu Ke, *J Mater Sci: Mater Electron*, 28 (2017) 987-993.
- [69] A. Balakrishna, O.M. Ntwaeaborwa, *Sens. Actuators B Chem.*, 242 (2017) 305–317.
- [70] R. Inoue, M. Kitagawa, T. Nishigaki, D. Morita, K. Ichino, H. Kusano, H. Kobayashi, *App. Surf. Sci.*, 142 (1999) 341-345.
- [71] M. Nogami, Y. Abe, *J. Sol–Gel Sci. Technol.*, 8 (1997) 867–870.
- [72] Y. Ni, C. Lu, Y. Zhang, Q. Zhang, Z. Xu, *J. Rare Earth*, 25 (2007) 94-98.
- [73] Peijing Tian, Jinshu Cheng, Gaoke Zhang, *Appl. Surf. Sci.*, 257 (2011) 4896-4900.
- [74] S.P. Porto, J.F. Scott, *Phys. Rev.*, 157 (1967) 716-719.
- [75] I.L.V. Rosa, A.P.A. Marques, M.T.S. Tanaka, D.M.A. Melo, E.R. Leite, E. Longo, J.A. Varela, *J. Fluoresc.*, 18 (2008) 239-245.
- [76] V.M. Longo, A.T. de Figueiredo, A.B. Campos, J.W.M. Espinosa, A.C. Hernandez, C.A. Taft, J.R. Sambrano, J.A. Varela, E. Longo, *J. Phys. Chem. A*, 112 (2008) 8920-8928.

- [77] S. Vidya, S. Solomon, J.K. Thomas, *Phys. Status Solidi A*, 209 (2012) 1067-1074.
- [78] J.W. Yoon, C.J. Choi, D. Kim, *Mater. Trans.*, 52 (2011) 768-771.
- [79] J. Tauc, A. Menth, *J. Non-Cryst. Solids*, 8-10 (1972) 569-585.
- [80] F. Yang, Z. Yang, Q. Yu, Y. Liu, X. Li, F. Lu, *Spectrochim. Acta A*, 105 (2013) 626-631.
- [81] J. Sun, D. Ding, J. Sun, *Opt. Mater.*, 58 (2016) 188-195.
- [82] G.R. Dillip, P. Mohan Kumar, B. Deva Prasad Raju, S.J. Dhoble, *J. Lumin.*, 134 (2013) 333-338.
- [83] P. Kubelka, Munk-Aussig F. ZeitFür, *The Kubelka-Munk, Theory of reflectance, Technology Physik*, 12 (1931) 593.
- [84] L.S. Cavalcante, V.M.Longo, J.C. Sczancoski, M.A.P. Almeida, A.A. Batista, J.A. Varela, *Cryst. Eng. Comm.*, 14 (2012) 853-868.
- [85] A. Balakrishna, Vinod Kumar, Ashwini Kumar, O.M. Ntwaeaborwa, *J. Alloys Compds.*, 686 (2016) 533-539.
- [86] X.H. He, M.Y. Guan, Z.C. Li, T.M. Shang, N. Lian, Q.F. Zhou, *J. Am. Ceram. Soc.*, 94, (2011) 2483-2448.
- [87] W.F. Zhang, Z. Yin, M.S. Zhang, *Appl. Phys. A*, 70 (2000) 93-96.
- [88] B.C. Jamalaih, J.S. Kumar, A.M. Babu, T. Suhasini, L.R. Moorthy, *J. Lumin.*, 129(4) (2009) 363-369.
- [89] B.V. Rao, U. Rambabu, S. Buddhudu, *Mater. Lett.*, 61(2007) 2868-2871.
- [90] G. Jia, Y. Song, M. Yang, Y. Huang, L. Zhang, *Opt. Mater.*, 31 (2009) 1032-1037.
- [91] K. Gayatri Sharma, Th. Prasanta Singh, N. Rajmuhon Singh, *J. Alloys Compds.*, 602, (2014) 275-280.
- [92] E.H. Song, W.R. Zhao, G.X. Zhou, X.H. Dou, C.Y. Yi, *J. Rare Earths*, 29 (2011) 440-443.
- [93] F. Wang, B.J. Chen, H. Lin, E.Y.B. Pun, *J. Quant. Spectrosc. Radiat. Transfer*. 147 (2014) 63-70.
- [94] F. Fu, B. Chen, L. Shen, E. Yu, B. Pun, H. Lin, *J. Alloys Compds*, 582 (2014) 265-272.

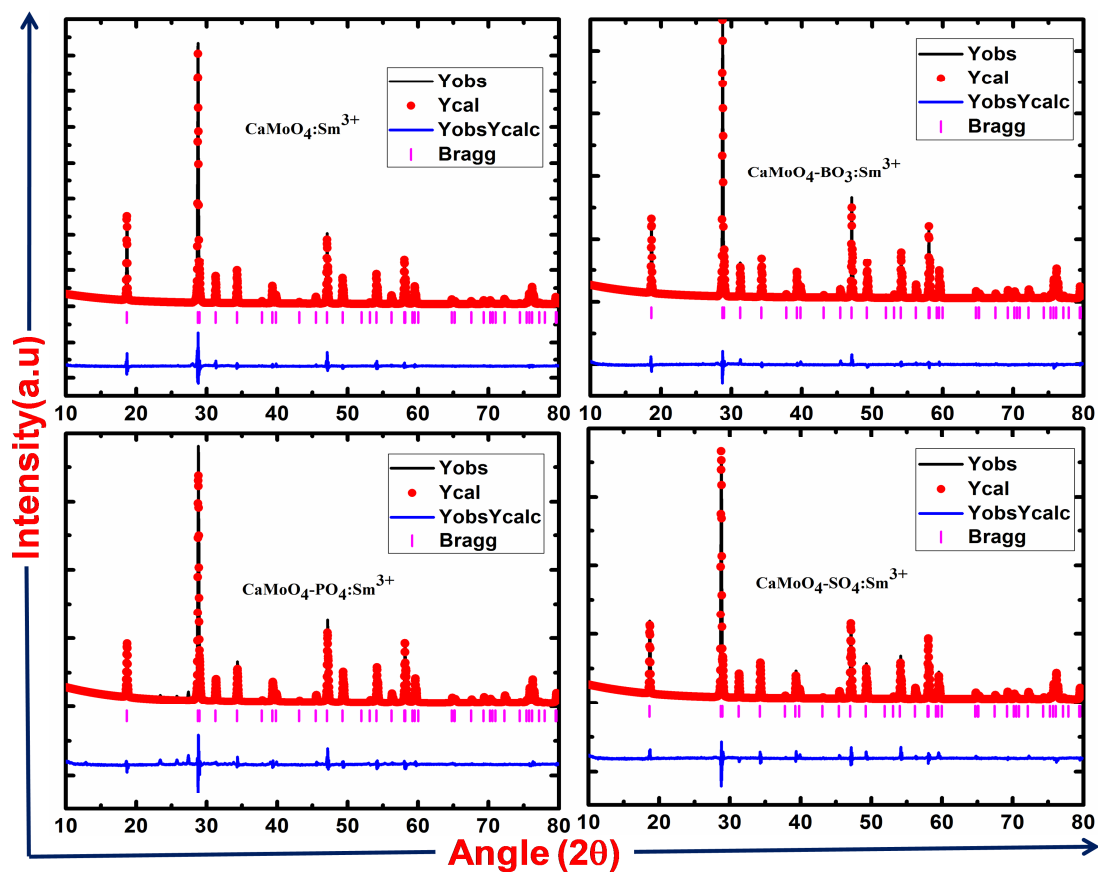


Fig. 1: Rietveld analysis of different CaMoO_4 phosphors substituted with anionic group systems (BO_3^{-3} , PO_4^{-3} and SO_4^{-2}).

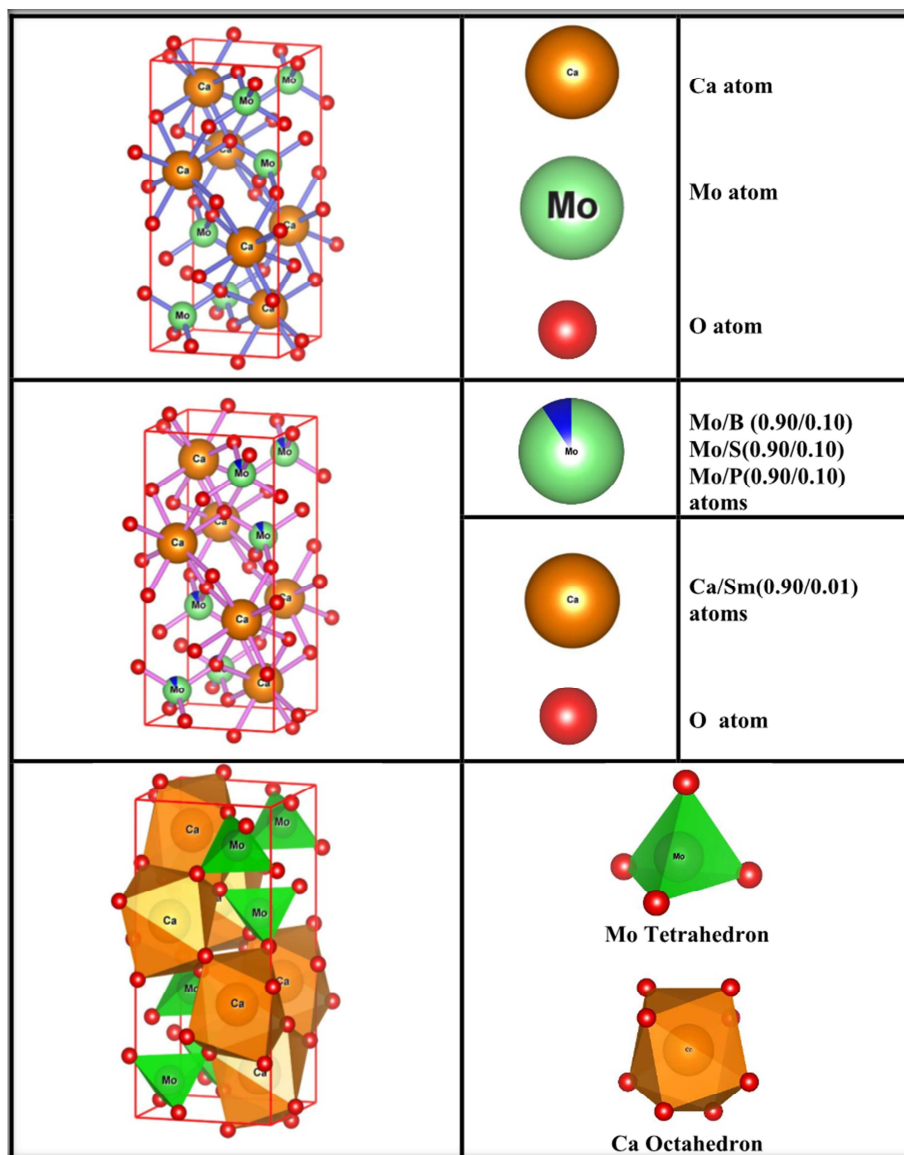


Fig. 2: Unit cell sheelite tetragonal structure of the CaMoO_4 crystal-partial substitution of different anionic groupic systems (BO_3^{-3} , PO_4^{-3} and SO_4^{-2}).

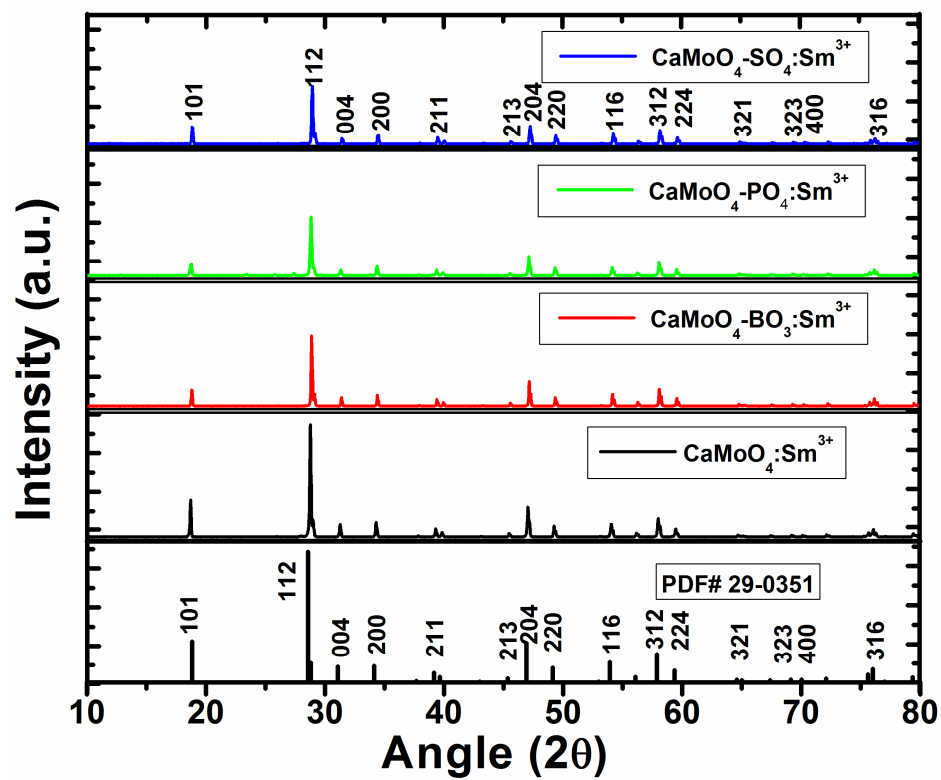


Fig. 3: The full XRD patterns of $\text{CaMoO}_4:\text{Sm}^{3+}$, $\text{CaMoO}_4\text{-BO}_3:\text{Sm}^{3+}$, $\text{CaMoO}_4\text{-PO}_4:\text{Sm}^{3+}$ and $\text{CaMoO}_4\text{-SO}_4:\text{Sm}^{3+}$ phosphors.

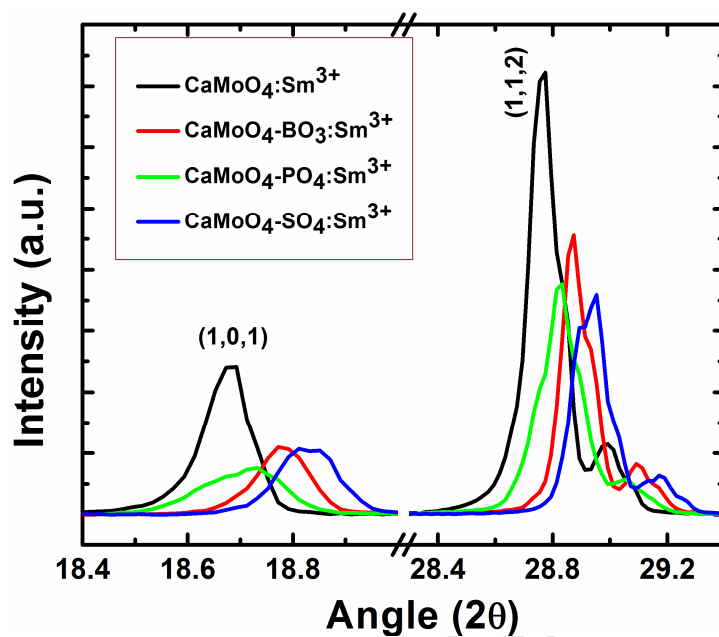


Fig. 4: The enlarged version of 101 and 112 diffraction peaks in the XRD patterns of $\text{CaMoO}_4:\text{Sm}^{3+}$, $\text{CaMoO}_4\text{-BO}_3:\text{Sm}^{3+}$, $\text{CaMoO}_4\text{-PO}_4:\text{Sm}^{3+}$ and $\text{CaMoO}_4\text{-SO}_4:\text{Sm}^{3+}$ phosphors.

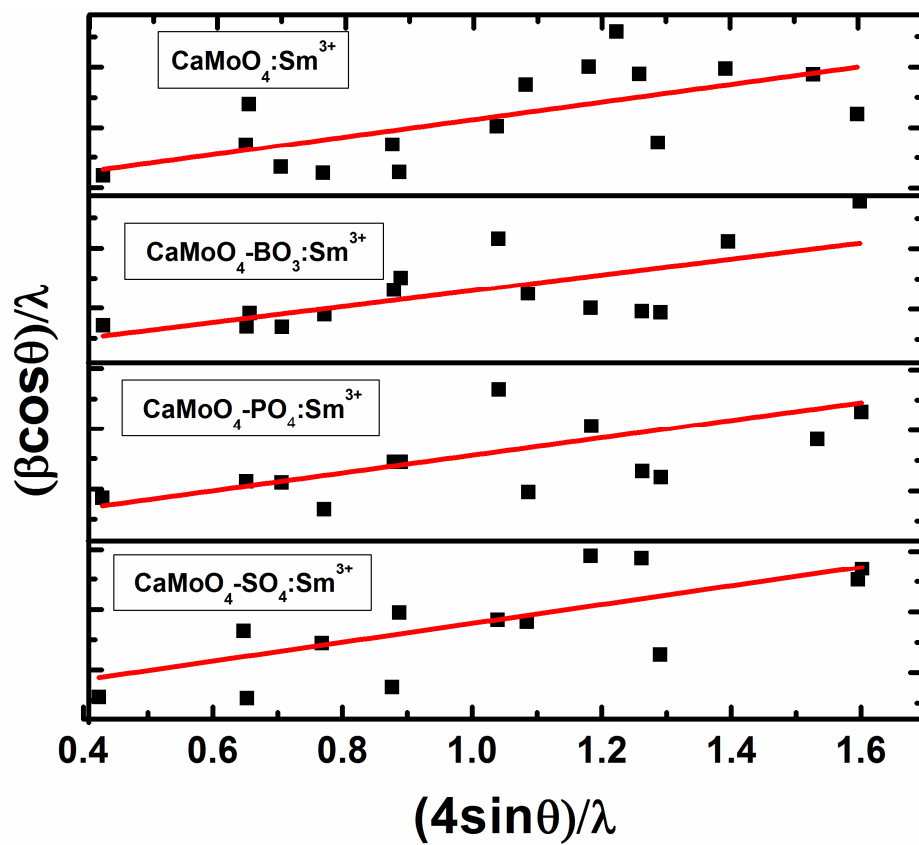


Fig 5: W-H plots of the four different $\text{CaMoO}_4:\text{Sm}^{3+}$ phosphors.

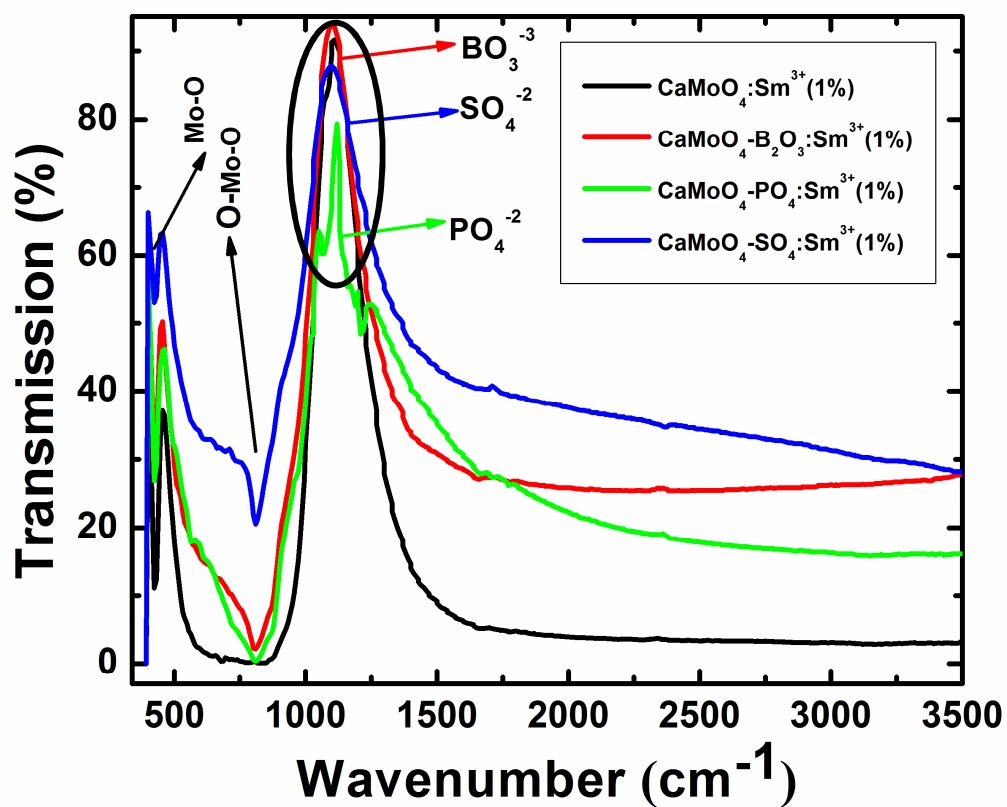


Fig. 11: The FT-IR spectra of different $\text{CaMoO}_4:\text{Sm}^{3+}$ phosphors substituted with anionic groups.

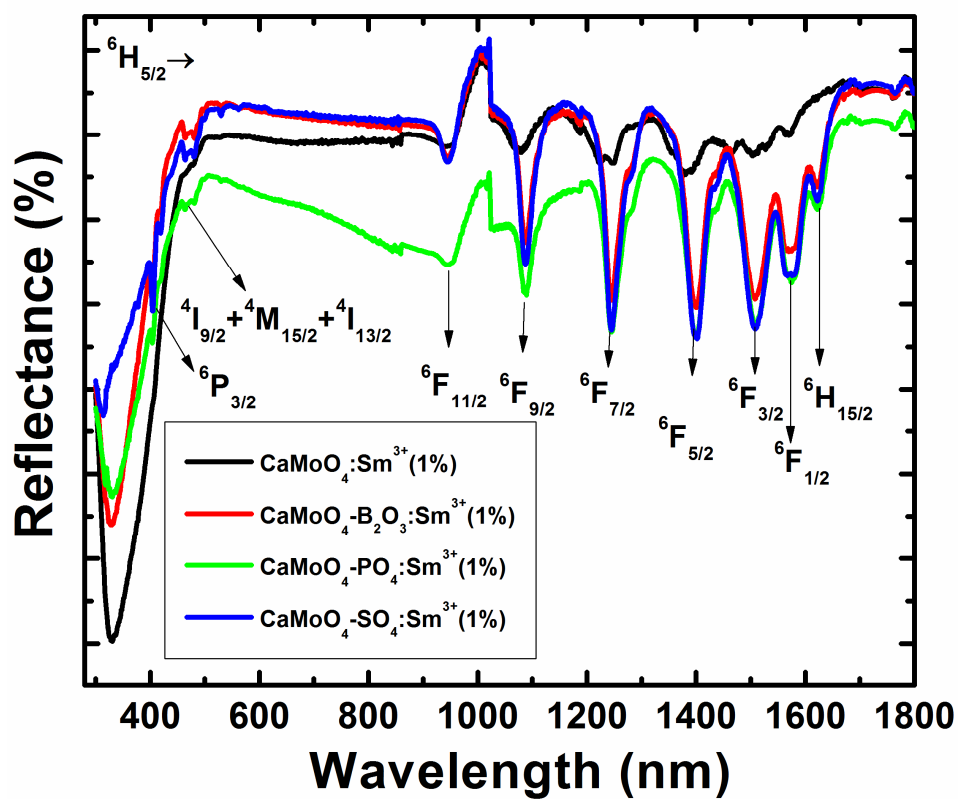


Fig. 12: The diffuse reflectance spectra (DRS) measured of the different $\text{CaMoO}_4:\text{Sm}^{3+}$ phosphors in the spectral region of 300-1800 nm.

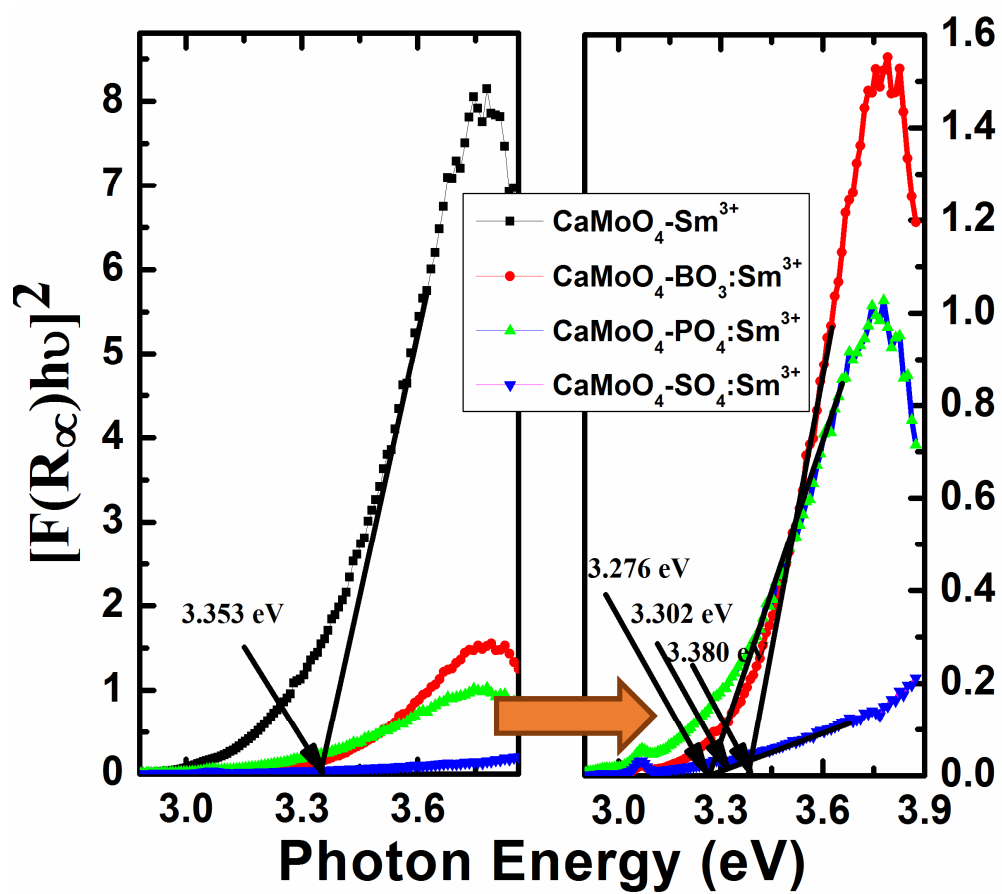


Fig. 13: The evaluated steep absorption edges in the range of 3.0–3.4eV for the four different $\text{CaMoO}_4\text{:Sm}^{3+}$ phosphors.

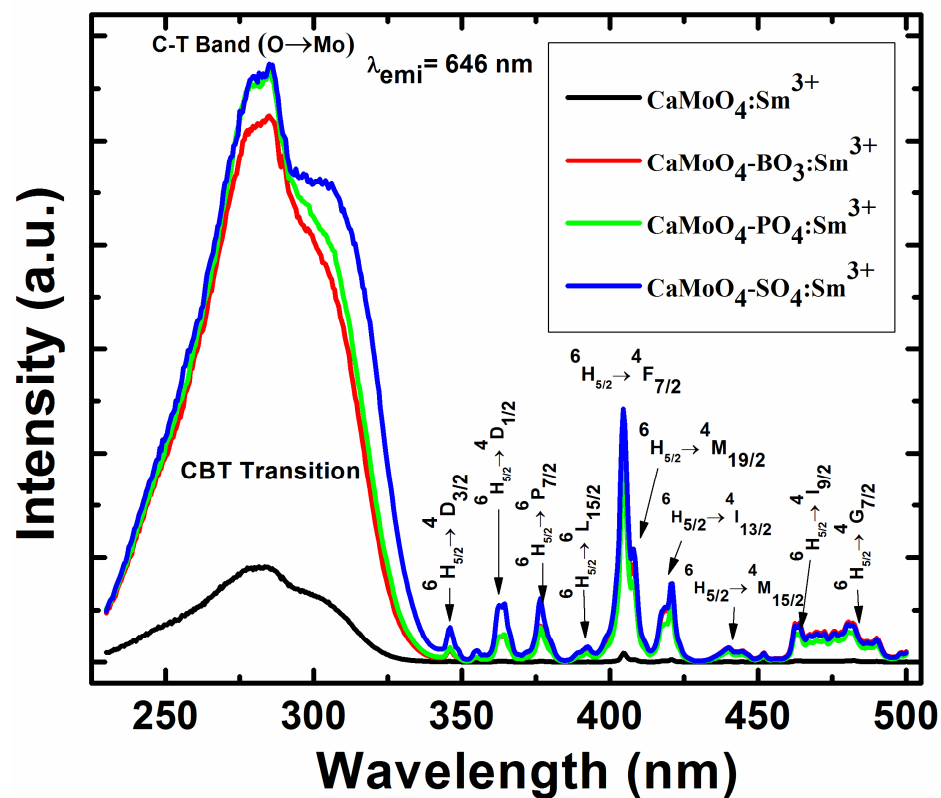


Fig. 14: The PL excitation (PLE) spectra recorded when monitoring the ${}^4G_{5/2} \rightarrow {}^6H_{9/2}$ emission peak of Sm^{3+} ion at 646 nm for the four different $\text{CaMoO}_4:\text{Sm}^{3+}$ phosphors.

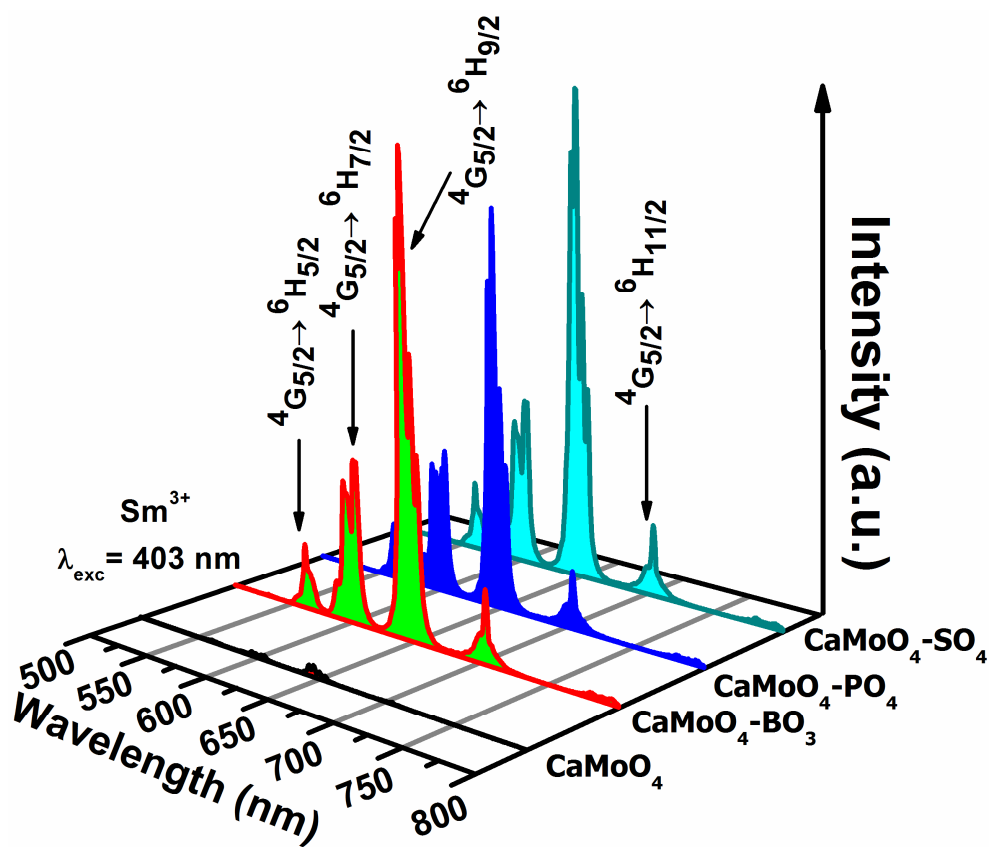


Fig. 15: The PL emission spectra of the different $\text{CaMoO}_4:\text{Sm}^{3+}$ phosphors substituted with SO_4^{2-} , PO_4^{3-} and BO_3^{3-} anionic groups.

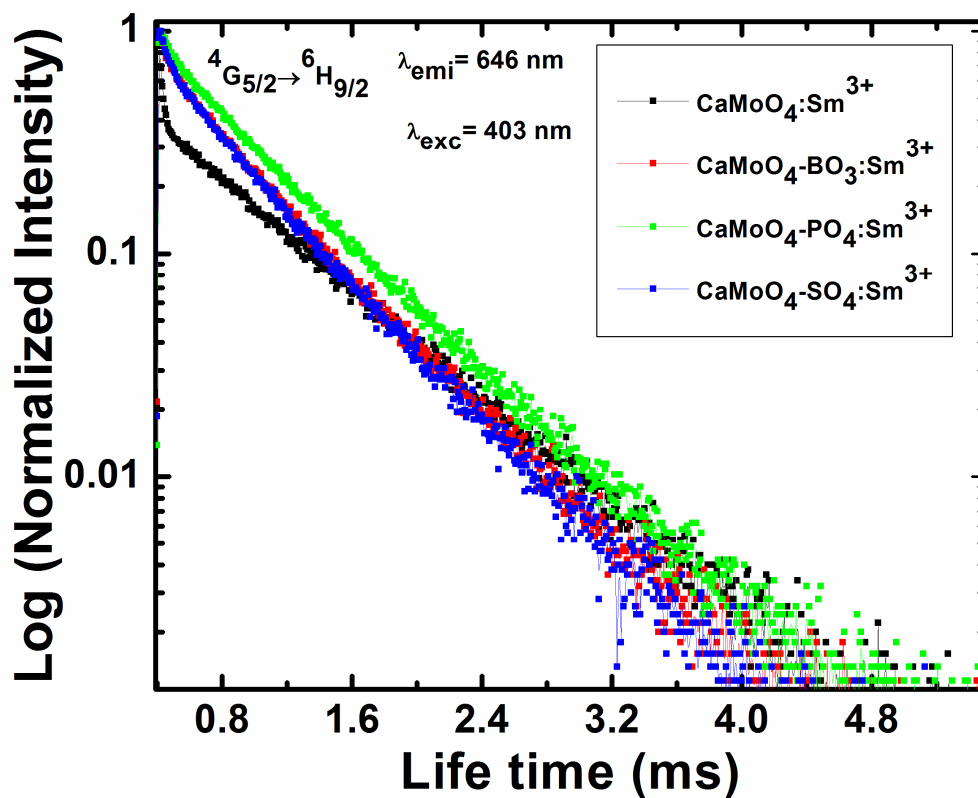


Fig. 16: The fluorescence decay curves of Sm^{3+} ion in different $\text{CaMoO}_4:\text{Sm}^{3+}$ phosphors substituted with anionic groups (BO_3^{-3} , PO_4^{-3} and SO_4^{-2}) by monitoring 646 nm from the transitions of ${}^4\text{G}_{5/2} \rightarrow {}^6\text{H}_{9/2}$ under the excitation of 403 nm.

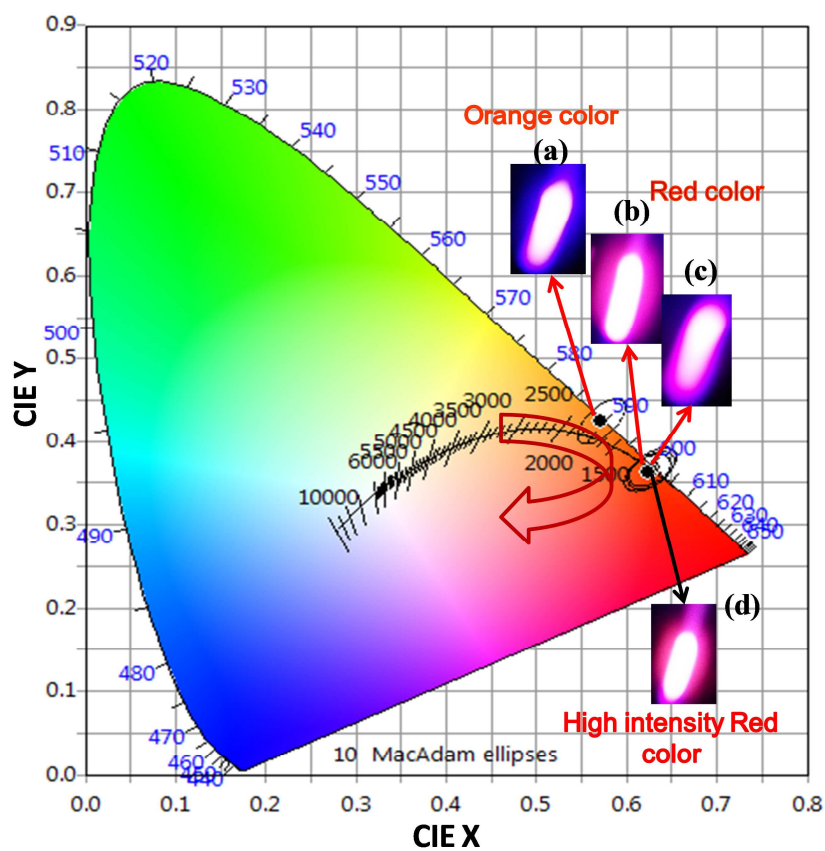


Fig. 17: CIE chromaticity coordinates of the $\text{CaMoO}_4:\text{Sm}^{3+}$ phosphors a) $\text{CaMoO}_4:\text{Sm}^{3+}$ b) $\text{CaMoO}_4\text{-BO}_3:\text{Sm}^{3+}$, c) $\text{CaMoO}_4\text{-PO}_4:\text{Sm}^{3+}$ and d) $\text{CaMoO}_4\text{-SO}_4:\text{Sm}^{3+}$. The insets show the corresponding digital photographs of samples under the excitation of a 404 nm Xenon lamp

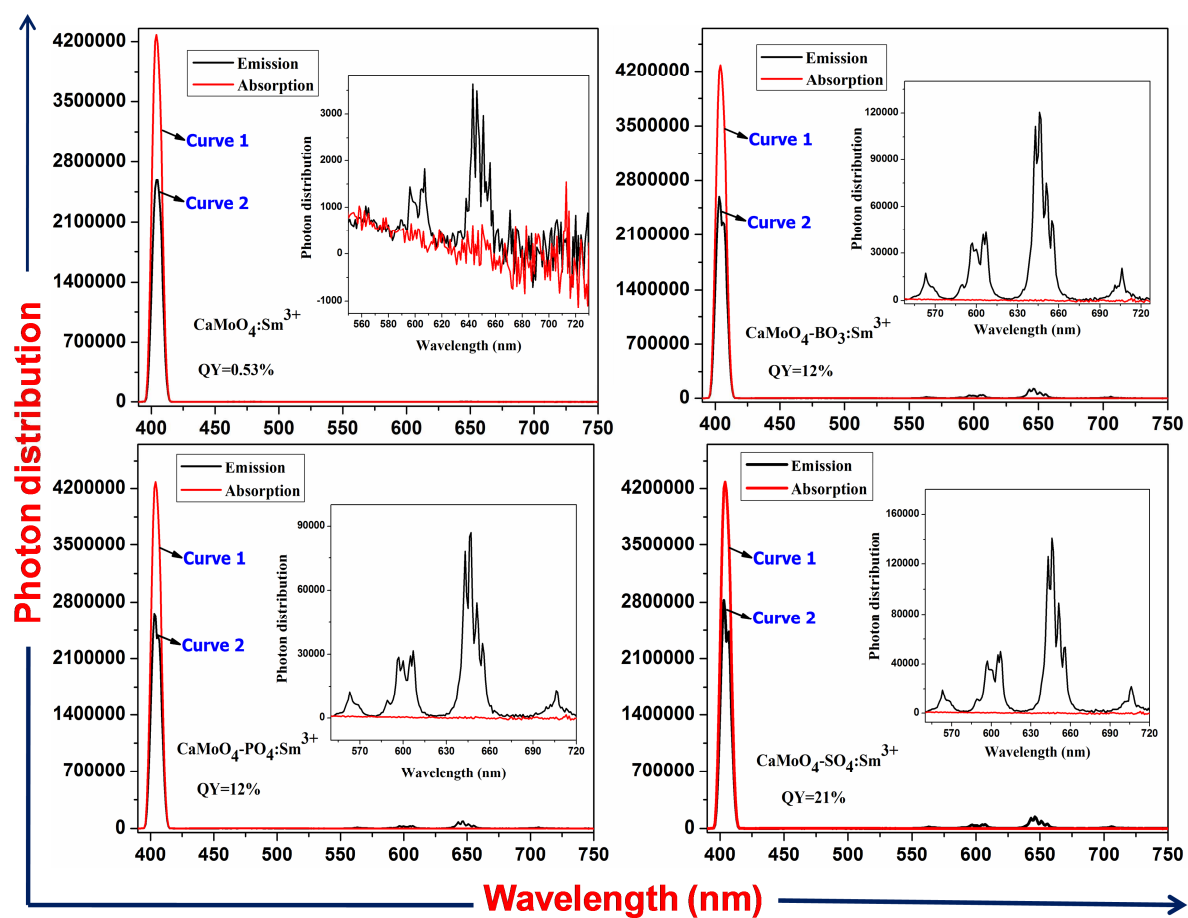


Fig. 18: Spectral power distribution of Sm^{3+} ion in different $\text{CaMoO}_4:\text{Sm}^{3+}$ phosphors substituted with anionic groups.

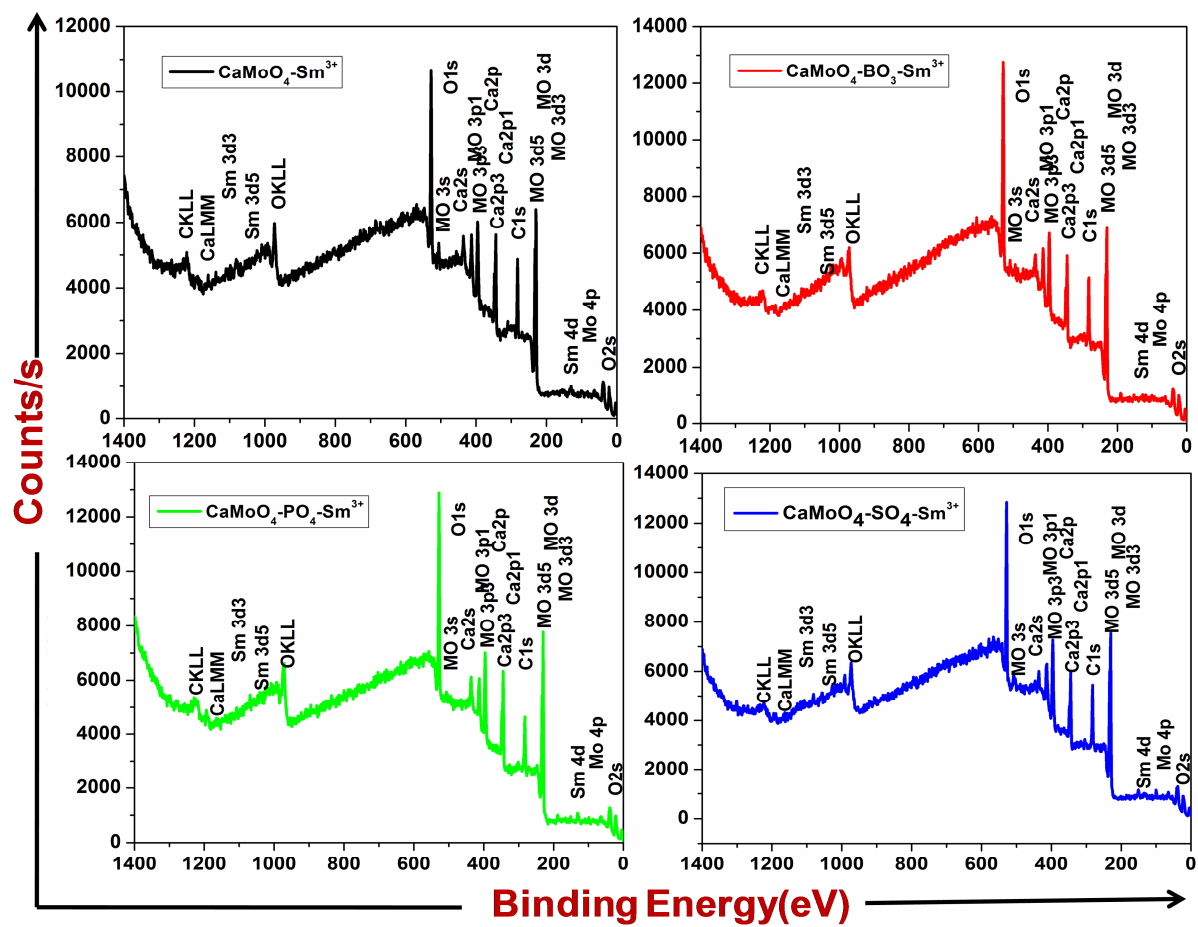


Fig. 6: XPS survey scan spectra of different $\text{CaMoO}_4:\text{Sm}^{3+}$ phosphors substituted with different anionic groups.

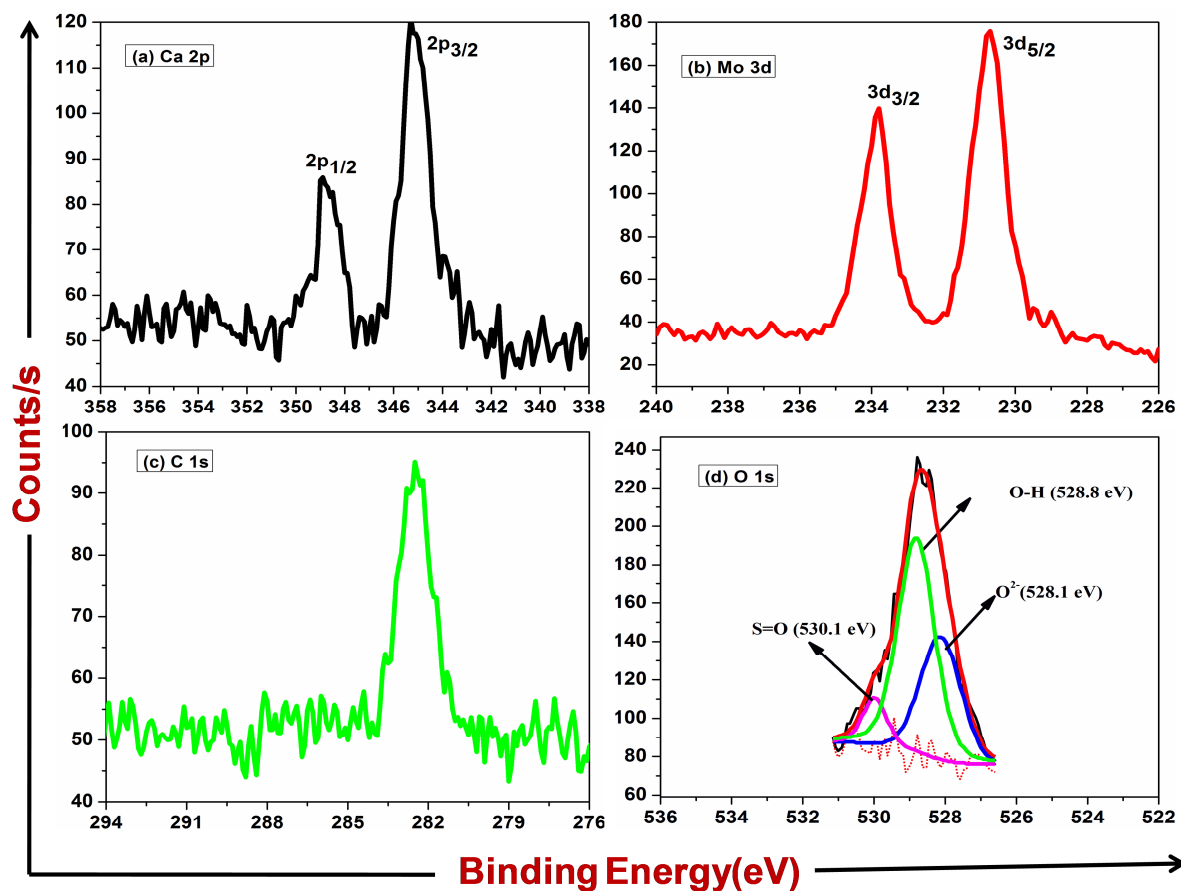


Fig. 7. The high resolution XPS scan spectra of (a) Ca 1s (b) Mo 3d (c) C 1s and (d) O 1s for the $\text{CaMoO}_4\text{-SO}_4\text{:Sm}^{3+}$ phosphors. Gaussian fit of O 1s is shown in (d).

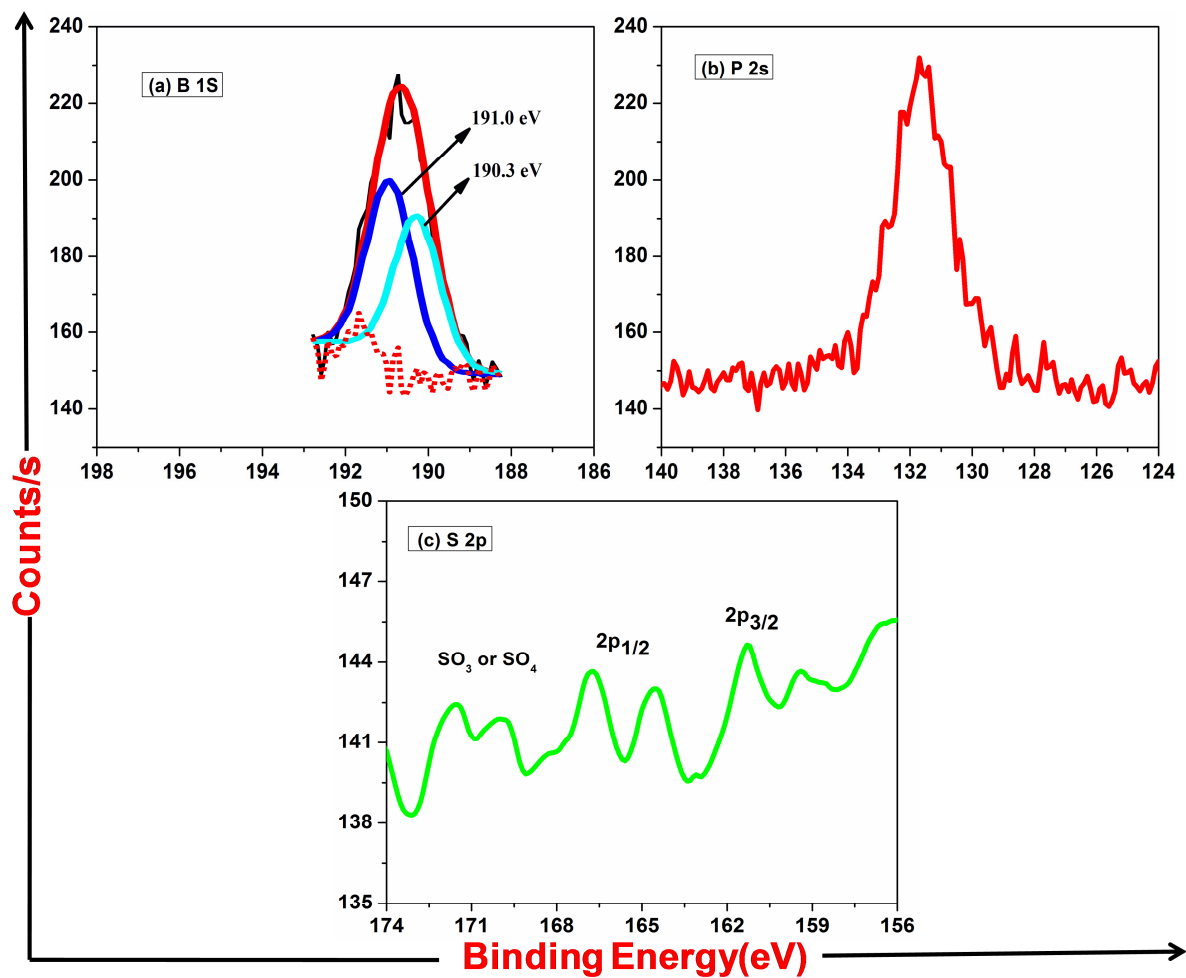


Fig. 8: The high resolution XPS spectra of (a) B 1S (b) P2s and (c) S 2p

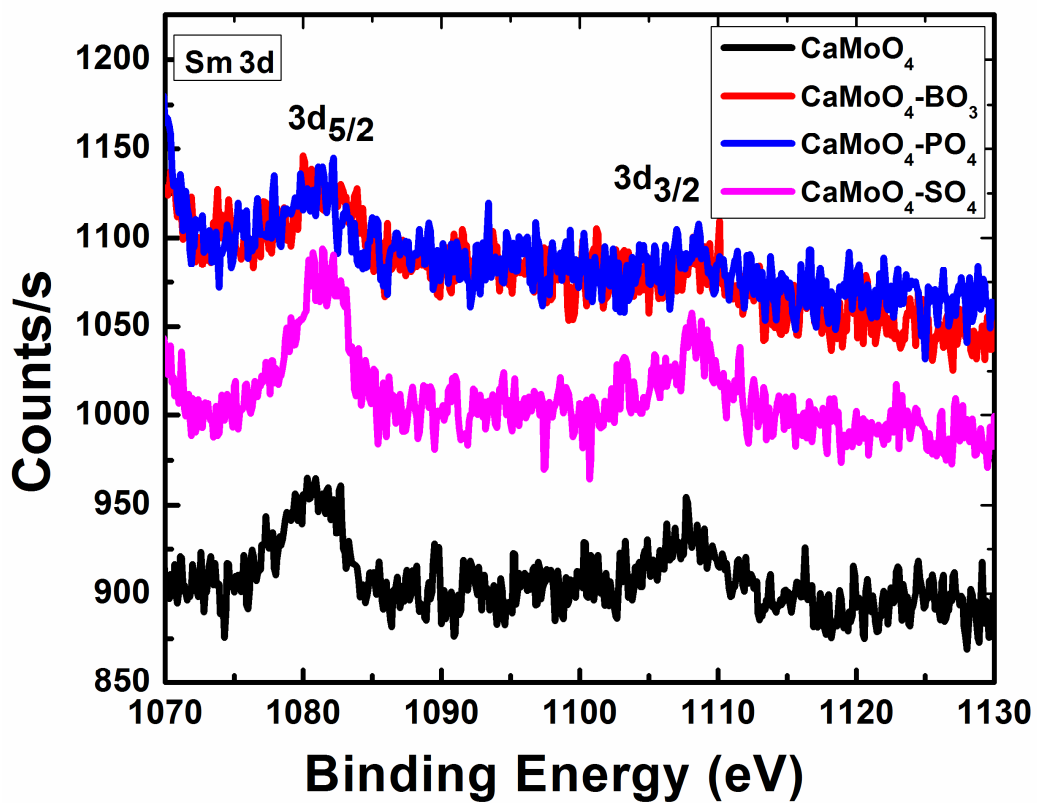


Fig. 9: High resolution XPS Sm 3d spectrum

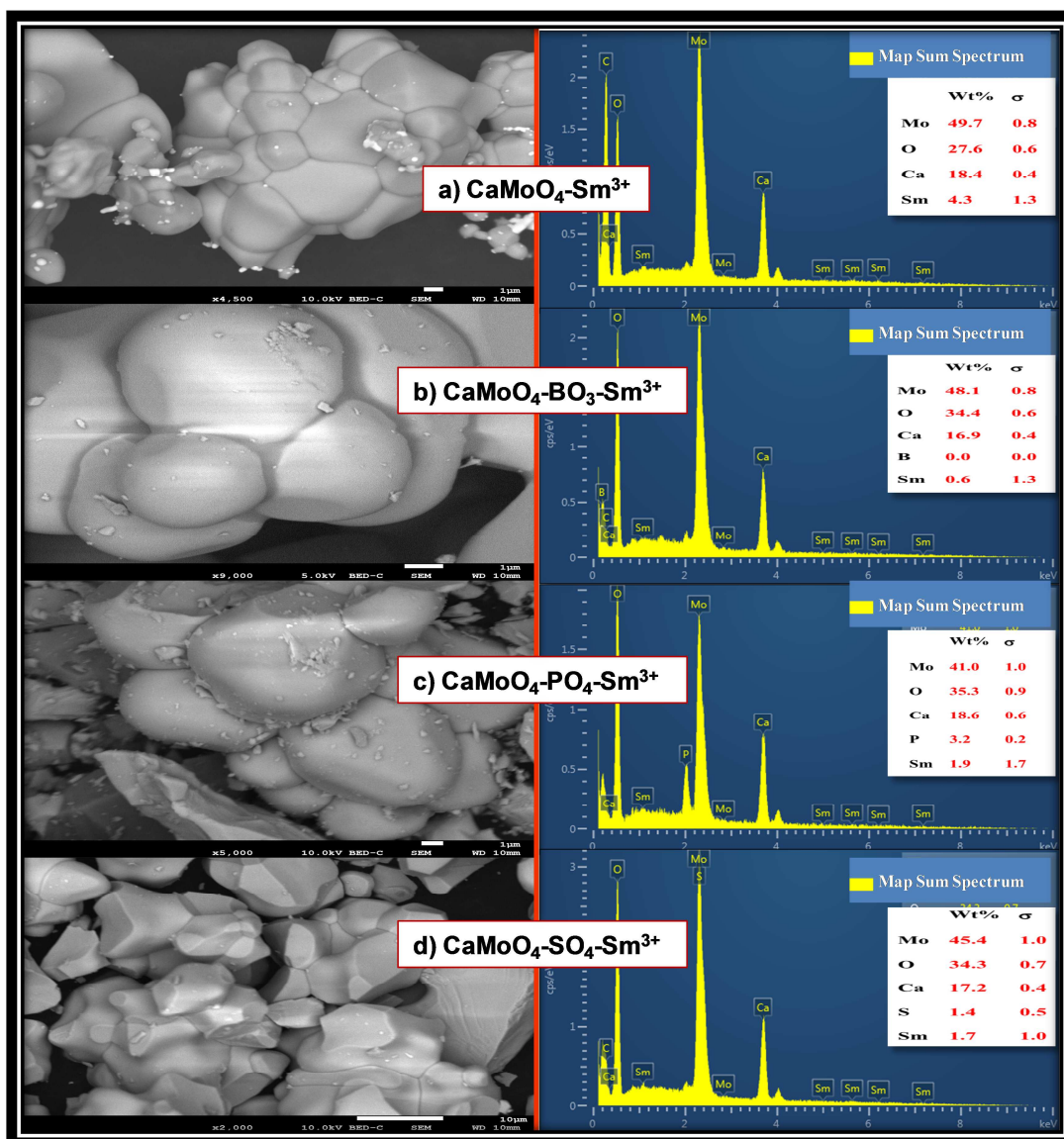


Fig. 10 (a), (b), (c) and (d): The SEM images and EDS spectra of different $\text{CaMoO}_4:\text{Sm}^{3+}$ phosphors substituted with anionic groups.

Highlights

- $\text{CaMoO}_4:\text{Sm}^{3+}$ was substituted with anionic groups (BO_3^{-3} , PO_4^{-3} and SO_4^{-2}).
- PL indicated that all of them can be effectively excited by 404 nm.
- Orange-red tuneable emission has been achieved by the substitution.
- $\text{CaMoO}_4\text{-SO}_4:\text{Sm}^{3+}$ phosphor showed the strongest PL emission.
- Potential candidates for UV excited red emission LED applications.